MODELING FUTURE HYDROLOGIC EXTREMES, FLOOD HAZARDS, AND EXPOSURE UNDER A HIGH EMISSIONS SCENARIO IN THE NEUSE RIVER WATERSHED

Hunter Carey Quintal

A thesis submitted to the faculty at the University of North Carolina at Chapel Hill in partial fulfillment of the requirements for the degree of Master of Science in the Department of Earth, Marine, and Environmental Sciences in the College of Arts and Sciences.

Chapel Hill
2022

Approved by:
Antonia Sebastian
Tamlin Pavelsky
Emily Eidam
Kathie Dello

ABSTRACT

Hunter Carey Quintal: Modeling Future Hydrologic Extremes, Flood Hazards, and Exposure under a High-Emissions Scenario in the Neuse River Watershed
(Under the direction of Antonia Sebastian)

Flood prone communities often lack predictive hazard maps necessary to inform public policy and efforts aimed at reducing household risks. This study evaluated the independent and combined effects of future climate and land use change scenarios on hydrologic response. I modeled changes in peak flows, volume, and timing between 2020 and 2100 using a large-scale (16,148 km^2) physics-based distributed hydrologic model of the Neuse River watershed and mapped the resulting flood depth and extent in Goldsboro, NC. I find that, in general, the effects of climate change on peak stream flow are greater than the effects of land use change; however, the role of land use change on discharge is spatially heterogeneous and dependent on localized patterns of land use change. In Goldsboro, the combined future climate and land use projections result in at least a five-fold increase in building exposure, with the greatest increases occurring for medium-sized storms.

To my fiancé, best friend, and PhT.
Thank you for your support over the last 8 years.

ACKNOWLEDGEMENTS

I would first like to acknowledge the North Carolina Water Resources Research Institute (NC WRRI) for their financial support and the opportunity to communicate the results of my research over the course of my master's degree. This included invitations to present my research at the 2021 NC WRRI Advisory Board Meeting, in a published news article on the NC WRRI website, and in my first oral conference presentation at the 2022 NC WRRI Annual Conference.

I would also like to acknowledge funding from the Martin Fellowship of the Department of Earth, Marine, and Environmental Science over the last two years for financial support that have been vital for my success at the University of North Carolina at Chapel Hill.

I would also like to acknowledge Dr. Kathie Dello and Dr. Shiela Saia at the North Carolina State Climate Office for introducing me to climate models and data analysis, and for their help acquiring and processing future climate data for my study location as I unintentionally entered the fray of this scientific discipline.

Finally, I am grateful to my advisor Dr. Antonia Sebastian and lab mate Lauren Grimley at the University of North Carolina at Chapel Hill for their inexhaustible guidance and technical support through the development, calibration, validation, and troubleshooting both a hydrologic and hydraulic model throughout this project. I'd also like to acknowledge the other members of the Watershed Hydrology and Flood Hazards Lab who have provided me with feedback on my practice presentations and have contributed to broader scientific discussions during lab group meetings.

TABLE OF CONTENTS

LIST OF TABLES

LIST OF FIGURES

LIST OF ABBREVIATIONS

3DEP	3D Elevation Program
AEP	Annual Exceedance Probability
CC	Climate Change
CMIP5	Coupled Model Intercomparison Project 5
DEM	Digital Elevation Model
EPA	Environmental Protection Agency
FEMA	Federal Emergency Management Agency
GEVD	Generalized Extreme Value Distribution
GCM	Global Climate Model
gSSURGO	Gridded Soil Survey
HEC-RAS	Hydrologic Engineering Center – River Analysis System
HUC	Hydrologic Unit Code
ICLUS	Integrated Climate and Land Use Scenarios
IPCC	Intergovernmental Panel on Climate Change
KWA	Kinematic Wave Approximation
LULC	Land Use Land Cover
LULCC	Land Use Land Cover Change
MRLC	Multi-Resolution Land Characteristics
MRMS	Multi-Radar Multi-Sensor System
NCORR	North Carolina Office of Recovery and Resilience
NED	National Elevation Dataset
NFIP	National Flood Insurance Program
NHD	National Hydrologic Database
NLCD	National Land Cover Database
NOAA	National Oceanic and Atmospheric Administration
NSE	Nash Sutcliffe Efficiency
NSSL	National Severe Storm Laboratory
RCP	Representative Concentration Pathway

RMSE	Root Mean Square Error
SSP	Shared Socioeconomic Pathway
USACE	United States Army Corps of Engineers
USDA	United States Department of Agriculture
USGS	United States Geological Survey

Introduction

In 2021, flooding was the most frequent, the deadliest, and, behind storms, the most financially damaging natural hazard globally, and scientists predict that they will pose exceedingly greater risks in the coming decades (CRED, 2022). Many drivers contribute to flood hazard propagation, including engineering, urbanization, urban sprawl, economic and social growth, and policy (Berndtsson et al., 2019); antecedent conditions and extreme precipitation (Kiem & Verdon-Kidd, 2013); and rural land management, river morphology and vegetation, and human behavior (O'Donnell & Thorne, 2020). However, climate change (CC) and land use-land cover change (LULCC) are thought to be two principle processes, along with hydraulic interventions, that disrupt the terrestrial hydrologic cycle and lead to flooding (Blöschl, 2022). Flood are attributed to changes in the magnitude and frequency of river floods globally over the last century (Bruno et al., 2021; Dottori et al., 2021; Winsemius et al., 2016).

Risk from flood hazards is traditionally communicated to the public using floodplain maps (Hagemeier-Klose & Wagner, 2009). In the United States, engineers and policymakers determine the 100-year floodplain to be a regulatory tool for defining flood hazards that correspond to standardized insurance premiums, land use policy and zoning ordinances, and future infrastructure and capital improvements. The 100-year floodplain defines the flood hazard extent and depth produced by a 100-year or 1% annual exceedance probability (AEP) precipitation event across the current landscape, where the 1% AEP precipitation event is an idealized hyetograph used to initiate a hydrologic and/or hydraulic model. In this case, the 1% AEP precipitation event is a storm that has a probabilistic magnitude calculated by the historic rainfall record. Floodplain map creation is also regulated, since the assumptions behind multiple hydrologic and hydraulic models can lead to diverging modeled flood hazards.

Contemporary floodplain maps can be powerful tools for limiting the exposure of vulnerable people and property to flood hazards. However, many maps are infrequently updated or may not exist for rivers in the United States, which ultimately can lead to their declining utility when they are not representative of current rainfall or land use inputs. Outdated maps do not only pose a risk of misinforming insurance, policy, and infrastructure planning efforts in the present day, but also further imperil community safety when used as the basis of future city and regional planning efforts. Unfortunately, this is a common reality (Hart & Halden, 2019). Therefore, short term planning goals fall short of addressing the risks posed by future climate and land cover on natural hazards (Ye et al., 2021). It is incumbent upon scientists to not only predict how flood hazard drivers such as CC and LULCC will influence the hydrologic cycle, but also determine how trends in river discharge exacerbate flood hazards over time.

Climate change and LULCC represent the influences that many of the flood hazard drivers above have on hydrological processes. Climate change alters the frequency and magnitude of storm events, which redistributes rainfall and results in runoff occurring more often (Gardner, 2009). LULCC alters the capacity for a landscape to attenuate streamflow by decreasing infiltration rates, limiting overland water storage capacity (Butler & Davies, 2011; Rogger et al., 2017), increasing the routing efficiency of runoff and discharge (Caldwell et al., 2012; Gori et al., 2019a; Sebastian et al., 2019), as well as stormwater conveyance into channels (Kaushal et al., 2017). When these two processes act in combination, their effects can compound and result in further increased runoff and discharge (Huq & Abdul-Aziz, 2021; Martin et al., 2017; Pumo et al., 2017; Suttles et al., 2018). Scientists expect peak discharge and timing to be modified in the coming decades in response to these drivers (Martin et al., 2017; O'Gorman & Schneider, 2009). There is growing interest in modeling hydrologic drivers to define flood hazards since people and property are increasingly affected when rivers more frequently exceed their bank full depth and spill into the floodplain.

Scientists expect the flood drivers of CC and LULCC to intensify at relatively faster rates across the U.S. Southeast. The 2017 National Climate Assessment suggests increases in the volume of the 20-year

return period storm by 9-13% in a less-likely, low emission scenario and by 12-21% in a more likely, high emission scenario by the late 21st century (Easterling et al., 2017; Reidmiller et al., 2018). Furthermore, Southeastern urban areas are expected to double by mid-century in response to population growth, and such urbanization and the resource requirements of a subsequently larger population will redefine land cover characteristics that alter the hydrologic cycle (Terando et al., 2014).

While many researchers have explored the impact of climate and land use change on discharge, only a handful have considered how the combination of these flood drivers exacerbate emerging streamflow patterns (Suttles et al., 2018; R. Wang et al., 2014). For example, Huq & Abdul-Aziz (2021) found that concurrent changes in urbanization and precipitation across southern Florida led to "synergistic, non-linear responses to runoff." This finding is important to note because researchers often model single flood hazard drivers or consider the addition of two model outputs to be sufficient for predicting their combined influence. However, research considering their amplifying effect finds that previous efforts underestimate predicted discharge and subsequent flood hazards (Akter et al., 2018). Additionally, hydrologists often neglect to assess the impact of accelerated streamflow trends on flooding, which limits understanding of the scale of changing natural hazard and science communication efforts. In the U.S. Southeast, where wide floodplains and slowly draining streams dominate the landscape (Gori et al., 2019a), recent trends in CC and LULCC belie the importance of quantifying their impact on flood hazards. In this study, I examine a large (HUC-6) river watershed in eastern North Carolina, the Neuse River, that drains the Raleigh-Durham triangle region and several cities downstream. My goal is to identify streamflow peak and floodplain extent to inform land use planning over the 21st century.

Background

Globally, flooding is the costliest natural hazard, accounting for more than 40% (2.8 billion USD) of direct damages from 1900 to 2015 (Daniell et al., 2016; Pricope et al., 2022). While global flood risk is predicted to continue to increase overall, flood risk is highly variable and dependent on both the social

and physical processes that affect the natural and built environment (Winsemius et al., 2016). The drivers of changing flood risk include impervious surfaces, urbanization, land use change, and climate change (Berndtsson et al., 2019). Researchers note that infrastructure, policy, and individual behaviors can have large impacts on curtailing flood hazards in the long term. Previous work has considered the impacts of both land use change and climate change on flood hazards separately. When holding climate constant, urbanization by 2030 will result in 2.7 times more inhabited areas being exposed to current day flood hazards as coastal metropolitan regions continue to emerge globally (Güneralp et al., 2015). When holding land use constant, the current 1% AEP flood will occur at least twice as often across 40% of the global land surface by 2050 and result in an ~187% increase in global flood risk over the flood risk predicted in the absence of climate change (Arnell & Gosling, 2016). Such climate change would double the flood frequency for ~450 million people and 430,000 km^2 of cropland.

In the United States, flooding is the most common natural hazard, where flood damages increased from $1.76 to $4.4 billion in 1997 dollars over the 20th century (Birkland et al., 2003). Currently, FEMA predicts that 13 million people live within the 1% AEP floodplain in America; however, researchers suggest that this number could be as much as 41 million (Wing et al., 2018). Projecting into the future, the 1% AEP precipitation event may further increase in both magnitude (~20%) and frequency (~200%), resulting in an increase in population exposure by 30-127% by the end of the 21st century (Swain et al., 2020). Despite knowledge of these global and national trends, locally, reliable and detailed quantitative projections of flood hazards are difficult to obtain for the past and present and are virtually impossible to obtain for the future (Kundzewicz et al., 2019). As such, practitioners, elected officials, and the public can benefit from projections of trends in hydrology and flood hazards that consider the influence of climate change and land use/land cover change.

Land cover is crucial for understanding streamflow and flood hazard projections because landscape surface features facilitate infiltration and runoff processes from storm events (Bedient et al., 2008). Land cover classifications are determined by anthropogenic land uses, which include cropland, pasture, forest,

range, and urban uses (Sohl et al., 2016). Generally, surface runoff and river discharge increase as a function of declining natural vegetation, where forest and high-density urban land cover define the endmembers of this negatively correlated relationship (Foley et al., 2005). Land covers that capture stormwater and slowly release runoff and shallow groundwater to stream channels are particularly adept at attenuating episodic stormwater. In the Southeast US, land use conversions to more impervious surfaces will impact flood hazards by increasing the duration and frequency of flooding events (Bradshaw et al., 2007). While changing land uses depend on the magnitude and context of human activity, spatially heterogeneous land use predictions remain uncertain since their underlying drivers are complex and are largely governed by spatiotemporal population growth trends (Sohl et al., 2016).

Population growth not only changes regional resource demands that drive land use changes but also increases flood hazard exposure when new urban and suburban development encroaches on the floodplain. The Southeastern US has been characterized by swift population growth since the mid-20th century and experienced the largest net population growth nationally in the late-20th century (Conroy et al., 2003). The population in NC grew by more than 60% between 1980 and 2010 (Census, 2010; O'Driscoll et al., 2010) and an additional 10% (900,000 people) between 2010 and 2020 (Census, 2021). Moreover, the population of NC is projected to grow by an additional 32% by 2050 (NCOSBM, 2022). This population growth will fuel further urban land cover, which is projected to increase between 101-192% by 2060 and produce a contiguous 'megalopolis' between Atlanta, GA and Charlotte, NC (Terando et al., 2014). Juan et al. (2020) and Gori et al. (2019a) model how LULCC in the rapidly urbanizing Houston, TX region has and may change probabilistic floodplain extent in the recent past and near future. Gori et al. (2019a) found that the 1% AEP floodplain area may increase by 13% between 2011 and 2050 and would result in an increase of 19% of exposed buildings to flood hazards solely in response to urbanization. Juan et al. (2020) found that by channelizing a river, the 1% AEP floodplain extent increases by 59% between 2011 and 2040 whereas a nearby non-channelized river's floodplain extent

increases by 3% over the same period. Trends in population growth across the US Southeast will potentially exacerbate flood hazards in suburban and urbanizing regions (Shepherd, 2005).

Urbanization modifies land surfaces by reducing vegetation, compacting soils, and decreasing their permeability. Urban landscapes impact runoff processes because smooth, impermeable surfaces across urban landscapes are more hydraulically efficient at transporting stormwater runoff (Berndtsson et al., 2019; Chen et al., 2017; Walsh et al., 2005). Impervious surfaces contribute to increases in runoff volume and higher peak flow, lower baseflow, and a decoupling of overland and channel water routing processes across storms of varying intensity (Boggs & Sun, 2011; O'Driscoll et al., 2010; Suriya & Mudgal, 2012). Less water can infiltrate the soil when construction activities have compacted the surface. For example, Gregory et al. (2006) found that infiltration rate declined as soils became compacted across natural forests (377-634 mm/hr reduced to 8-175 mm/hr), planted forests (637-652 mm/hr reduced to 160-188 mm/hr), and pasture sites (225 mm/hr reduced to 23 mm/hr). The timing of a flood can also shift to earlier in a storm when rainfall is unable to infiltrate into soils because runoff reaches channels earlier (S. Brody et al., 2014). For example, Huang et al. (2008) found that as impervious surface increased from 5 to 13% of a Taiwanese watershed area, time to peak discharge declined from 11 to 6 hours and peak flow increased from 127 to 629 cms under varying storm events. Ogden et al. (2011) found that impervious surface becomes less important for determining runoff efficiency and volume as storm magnitude becomes more extreme (<1% recurrence interval).

Knowledge of climate patterns is important for predicting streamflow and flood hazards, especially in urbanizing regions since rainfall is the leading driver of future urban flood risk (O'Donnell & Thorne, 2020; Sun et al., 2002). Changes in precipitation from 1988 to 2017 have contributed to more than 1/3 ($73 billion) of cumulative flood damages across the US (Davenport et al., 2021). As flooding is already the costliest natural hazard, it is imperative to understand how future storm magnitudes and frequencies will affect watershed hydrology and flood hazards (Slater et al., 2021). Future precipitation is difficult to predict because of the complexity of climate drivers and feedbacks and non-stationarity in the climate

system, which further makes modeling efforts difficult because model variability responds to time horizon and projection scenario (Dottori et al., 2018; Gupta et al., 2013; Knutti & Sedláček, 2013; Liu et al., 2014; Milly et al., 2008; Steinschneider et al., 2015; C. Wang et al., 2014). However, researchers still explore how climate and socioeconomic scenarios will influence flood hazards. Swain et al. (2020) found that the 1% AEP precipitation event under an RCP 8.5 scenario would result in a 20% increase in storm volume and a doubling in storm frequency across the US that would increase population exposure between 30-127%. Mohanty & Simonovic (2021) furthered this research by modeling the effects of CC on floodplain extent. They found an increase in flood inundation extent by over 30% for the 1% AEP flood in the near- (2021-2060) and far- (2061-2100) periods solely by the influence of CC predicted by CMIP6.

In recent years, researchers have reached a consensus that warming temperatures are leading to a global intensification of the hydrologic cycle and will result in more severe extreme flooding and droughts (Archfield et al., 2016; Carter et al., 2018; Easterling et al., 2017; Hirabayashi et al., 2013; Hodgkins et al., 2017; Kunkel et al., 2020; Reidmiller et al., 2018; Slater & Villarini, 2016; Wing et al., 2022). While droughts occur over extensive regions and on seasonal to annual time periods, flooding can be a sporadic natural hazard with magnitudes that vary greatly across relatively fine spatial scales. This scientific consensus underscores the need for research to identify where flooding is predicted to occur, not only now, but also in the near future. The predicted increase in the magnitude and frequency for a given probabilistic precipitation event will result in a deeper and wider floodplain and thereby increase flood exposure for buildings near the current floodplain (Pricope et al., 2022). This information can be obtained through modeling efforts and distributed and disseminated to those who are and those who are likely to become at risk. Direct modeling of flood hazards and exposure has been explored under LULCC (Gori et al., 2019a; Juan et al., 2020) and CC (Mohanty & Simonovic, 2021) independently, but less often are their combined effects on flood hazards considered (Huq & Abdul-Aziz, 2021; Martin et al., 2017; Suttles et al., 2018). This research seeks to understand the relative contribution of each flood driver individually and combined on flood hazard outcomes.

Data and Methods

Study Area

The Neuse River watershed is located in eastern North Carolina USA (Figure 1). The Neuse watershed drains 6235 mi^2 (16,148 km^2) from the Piedmont through the Coastal Plain and into the Pamlico Sound. The upper portion of the watershed is characterized by a large area of urbanization that surrounds the larger metropolitan area of Raleigh, NC (Frey, 2012). Seven cities are located along the Neuse River and seventy incorporated municipalities are located within the watershed. Land use changes in the watershed from 1992 to 2001 predominantly increased medium- to low-density urbanization (11%), animal agriculture (14%), and grasslands (2%) and decreased crop agriculture (15%), forest (9%), and wetland (3%) (Rothenberger et al., 2009).

The area is subject to frequent flooding, specifically extreme precipitation events and tropical cyclones. The watershed is also experiencing population growth, particularly around the state capitol of Raleigh, which is driving increases in urbanization, deforestation, and a transition from agricultural to industrial and commercial uses. These changes will influence the hydrologic processes of infiltration, floodplain storage, and routing efficiency, likely expanding floodplains in the future. High rates of change of these drivers in eastern North Carolina makes the Neuse River watershed an ideal location to study trends in watershed hydrology and flood hazards (Paerl et al., 2020; Terando et al., 2014).

This study focuses on fluvial flooding that arises during extreme rainfall events in the Neuse River watershed. Eastern North Carolina is particularly flood prone due to its wide, shallow floodplains which enable rapid increases in inundated area for a given increase in precipitation. Recent studies suggest that the frequency of high discharge events in eastern North Carolina has doubled since 1950 (Dethier et al., 2020). For example, Paerl et al. (2020) found aperiod of unprecedently high precipitation since the late 1990s representing a regime shift in extreme precipitation associated with tropical cyclone activity. Falls Dam was authorized for creation downstream of the Raleigh area under the Flood Control Act of 1965 to

mitigate downstream flooding, particularly along Goldsboro, Kinston, and New Bern, and operates with respect to bank full stream depth at Clayton, NC (USACE, 2013). Despite dam operations since 1983, the river continues to exhibit increases in the 90th percentile of flows (Meitzen, 2016). Ercan et al. (2020) found that average monthly surface runoff will increase within the Upper Neuse watershed between 9.8% (RCP 4.5) and 91.2% (RCP 8.5) due to the combination of a decrease in evapotranspiration and an increase in precipitation volume. If these trends continue, communities along the Neuse River can expect greater flood hazards in the future.

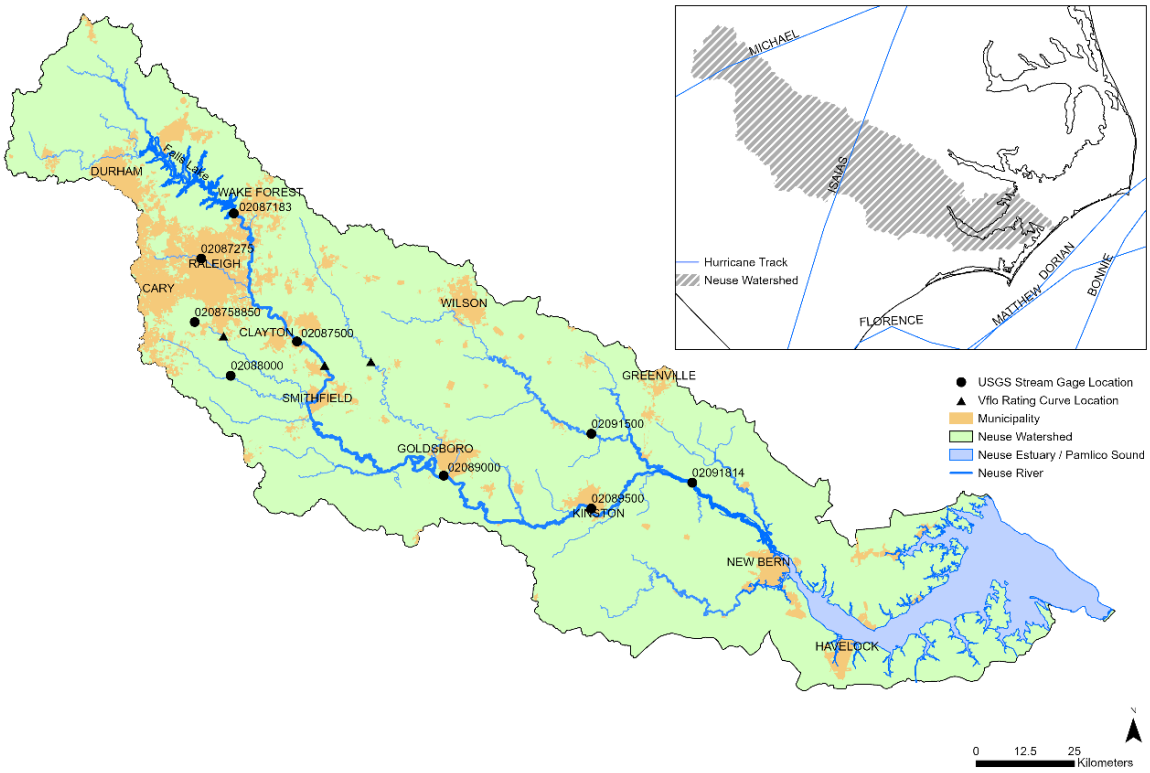

Figure 1. Map of Neuse River watershed. HUC 6 outline of the Neuse River watershed displaying the location of USGS stream gages, rating curves, cities within the watershed, and stream order as the Neuse flows southeast into the Neuse River Estuary and Pamlico Sound. Inset shows the location of the Neuse River watershed relative to the State of North Carolina USA and the paths of recent tropical cyclones that were used in model validation.

To demonstrate the influence of future changes in extreme discharge on floodplain extent, I examine the City of Goldsboro located along the Neuse River 45 miles (72 km) southeast of Raleigh, NC. Goldsboro experienced significant flooding during recent tropical storms including Hurricanes Fran (1996), Floyd (1999), Matthew (2016), and Florence (2018) (Doll et al., 2020). Three tributaries run through Goldsboro: Little River, Big Ditch (highly channelized and armored), and Stoney Creek. The United States Army Corps of Engineers (USACE) has developed detailed hydraulic models for these tributaries used to produce hazard maps for planning efforts as well as the National Floodplain Insurance Program (NFIP). Repeated flooding along the Neuse River has led the North Carolina Office of Recovery and Resiliency to identify three strategic buyout zones that aim to reduce current flood hazard exposure (Figure 1b). In addition, researchers are actively exploring adaptation and mitigation strategies within Goldsboro including flood control wetlands and water farming, which could reduce current and future flood exposure (Doll et al., 2020).

Model Framework

This study links projections of future land use and precipitation with hydrologic and hydraulic models to quantify changes in future flood hazards and building exposure. Figure 2 describes the model framework, which consists of the following components: 1) analysis of climate model output to produce future scenarios of extreme precipitation; 2) analysis of land use model output to produce future land use scenarios; 3) hydrologic modeling to quantify changes in watershed and tributary peak discharge, volume, and timing; and 4) hydraulic modeling to determine changes in water surface elevation and extent.

I obtain future land uses at decadal time steps for the period from 2020 to 2100 under the RCP 8.5 and the SSP 5 scenario. The shared socioeconomic pathways predict patterns of land development in response to challenges for mitigation and adaptation to the RCP scenarios (Pörtner et al., 2022). An RCP 8.5 and SSP 5 scenario represents a global economy that continues to emit greenhouse gases at greater rates (O'Neill et al., 2014). Statistically downscaled daily precipitation is obtained from Coupled Model Intercomparion

Project 5 (CMIP5) under the same RCP 8.5 scenario and processed to generate estimates of five AEP precipitation events: 20%, 10%, 2.0%, 1.0%, and 0.2%. I then use these future land use and climate scenarios to force a calibrated hydrologic model of the Neuse River Watershed, and evaluate their individual and combined influences on hydrologic response. To demonstrate the importance of these hydrologic changes on flood hazard and exposure at a city scale, the resulting discharge hydrographs are used as input to a 1D steady state hydraulic model to generate flood hazard maps for Goldsboro, NC. These maps are then compared against the predicted 2020 floodplain boundary for same AEP precipitation events described above (i.e., in 'the 2020 floodplain').

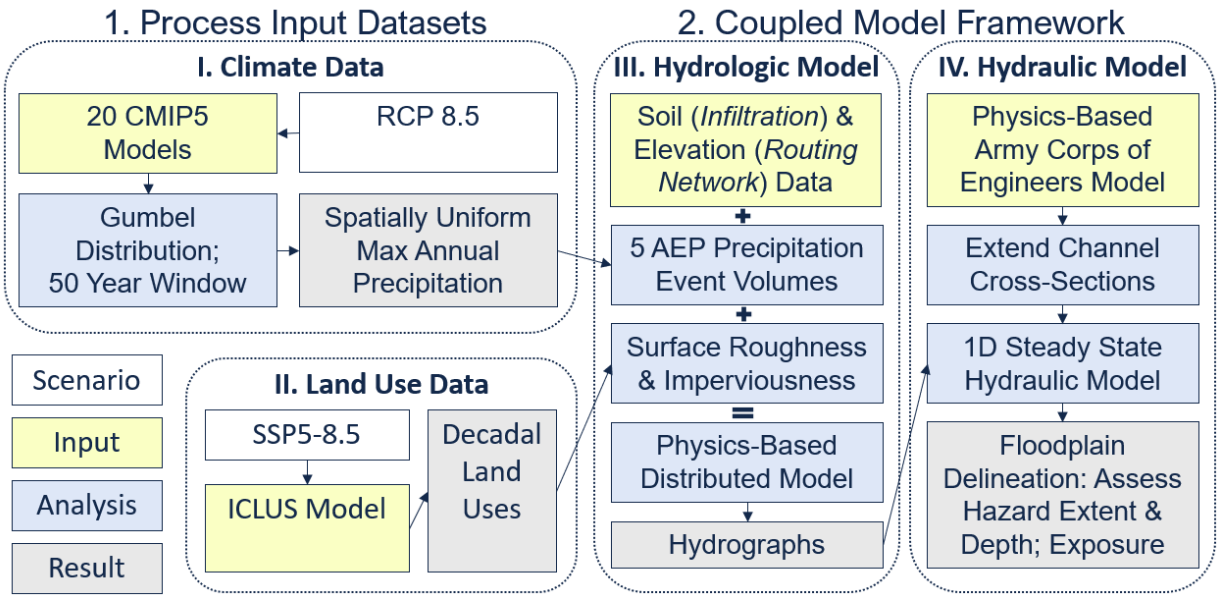

Figure 2. Coupled model framework. (I) assess climate data from 20 Global Climate Models under the RCP 8.5 scenario; (II) assess land use data from one model under the combined RCP 8.5 and SSP 5 scenario; (III) input these data into a hydrologic model to determine discharge hydrographs; and (IV) input hydrographs into a hydraulic model to define water depth and extent.

Future Climate Projections

Representative Concentration Pathway (RCP) scenarios are first described by the Intergovernmental Panel on Climate Change (IPCC) to predict the impact of future greenhouse gas

emissions on Earth system processes (IPCC, 2007). RCP 4.5 and RCP 8.5 are the two most commonly cited scenarios, representing increases in 4.5 W/m^2 and 8.5 W/m^2 of surface radiation. As such, RCP 4.5 is analogous to a business-as-usual scenario where global emissions continue at their current rate, albeit with the caveat that substantial policy change must first occur; while this is still possible, it is growing increasingly unlikely. RCP 8.5 represents both a worst-case and a closer to business-as-usual scenario where the global economy continues to industrialize and emit greenhouse gases at similar rates to already industrialized economies; however, this scenario may still overpredict future climate globally (Schwalm et al., 2020). The climate science community uses RCP 8.5 to represent the global climate trajectory and RCP 4.5 to describe what could occur given substantial policy change (Hausfather & Peters, 2020). For this thesis, I evaluate the RCP 8.5 scenario in light of the climate community's consensus and because of my interest in evaluating floodplain extent evolution under a worst-case future scenario (Allan & Soden, 2008; Sridhar et al., 2019).

CMIP5 is an effort to produce regional projections of multiple global climate models (GCMs) to determine variability in climate predictions. Three forms of uncertainty exist within GCMs and their byproducts (i.e. CMIP5): internal variability, model uncertainty, and scenario uncertainty (Hawkins & Sutton, 2009). Internal variability represents natural fluctuations of the global climate system, model uncertainty describes climate model responses to anthropogenic radiative forcing, and scenario uncertainty explains the scientific community's ability to predict atmospheric warming globally. These three uncertainties introduce biases into climate variable projections. For example, single climate research groups have developed multiple GCMs, which can introduce model uncertainty biases within 'model families' towards specific atmospheric processes (Steinschneider et al., 2015). Steinschneider et al. (2015) found that model family bias influences both the volume and probability of precipitation projections by as much as 20% in the United States by mid-century. As such, research that uses ensemble climate models are further biased towards the assumptions that a few climate research groups make about complex and dynamic atmospheric physics.

GCMs can either be statistically downscaled or dynamically downscaled for regional analysis (Barsugli et al., 2013; Dixon et al., 2016). One statistical downscaling approach developed by Livneh et al. (2013) is often cited in climate hindcast analyses since it enables climate projections at a 1/16° resolution, which is an improvement over the 1/8° resolution of similar methods. CMIP5 projections broadly agree that temperatures will become noticeably warmer. So too will precipitation increase, albeit at a slower rate than rising temperatures (Steinschneider et al., 2015). In North Carolina, CMIP5 models suggest that total annual precipitation will increase, and so too will extreme precipitation intensity and frequency increase (Kunkel et al., 2020; Pokhrel et al., 2020). These projections are in line with recent regional trends in the increasing frequency of heavy rainfall (Kunkel et al., 2020).

In this study, I consider climatic changes across the watershed using a 20 model CMIP5 ensemble provided by North Carolina State Climate Office (NCSCO). I predict daily total precipitation from 1950 to 2099 at a 4 km spatial resolution produced by the Multivariate Adaptive Constructed Analogs (MACA) statistical downscaling method (Abatzoglou & Brown, 2012). The MACA method uses a training historical dataset, provided by Livneh et al. (2013) in this case, to remove GCM model uncertainty biases. Additionally, MACA uses an analog approach to geospatially map GCM outputs to the highly variable, fine scale domain. This allows for a continuous record of predictive climate data that links the record of hindcast predictions (1950-2005) to the record of forecast predictions (2006-2099) using congruent approaches, resolutions, and climate variables (Aliyari et al., 2021; Turner et al., 2015).

I compile a continuous spatiotemporal record for each model of the watershed and conduct a spatial and statistical analysis of the data. This analysis first determines the annual maximum daily precipitation volume for each model and then calculates the volume of five AEP precipitation event storm using both a 30- and 50-year moving window approach (Figures 14 & 15) similar to Fagnant et al., (2020). I then fit these to a Gumbel Generalized Extreme Value Distribution (GEVD) (Schulz & Bernhardt, 2016). The Gumbel is often used to predict the probability that a natural hazard of a given magnitude will occur if there exists a robust record of event frequencies and magnitudes from which to sample (Gumbel, 1941),

and is often cited as appropriate for fitting future streamflow (Yue et al., 1999) and precipitation predictions in hydrologic studies (Koutsoyiannis, 2003).

Hydrologists consider a 30-year record to be sufficient for similar analyses because of data availability; however, a longer record will consequently improve confidence in the statistical probability of an events' recurrence interval or AEP, while not incorporating scale dependencies that occur on timescales larger than 50 years (Markonis & Koutsoyiannis, 2016; Yuan et al., 2019). Therefore, in this assessment, I use the results from the 50-year moving window analysis in the model framework. I link the historical dataset with the CMIP5 dataset to produce a continuous precipitation record across all 20 models from 1950 to 2100. This produced a continuous record of twenty 20%, 10%, 2.0%, 1.0%, and 0.2% AEP volumes for every year from 2000 to 2100, or one prediction per year per model. Ultimately, I chose to spatially average precipitation over the entire watershed. I believe it is reasonable to assume that the median volume for each year is representative across the entire watershed due to the uncertainty associated with statistical downscaling discussed above.

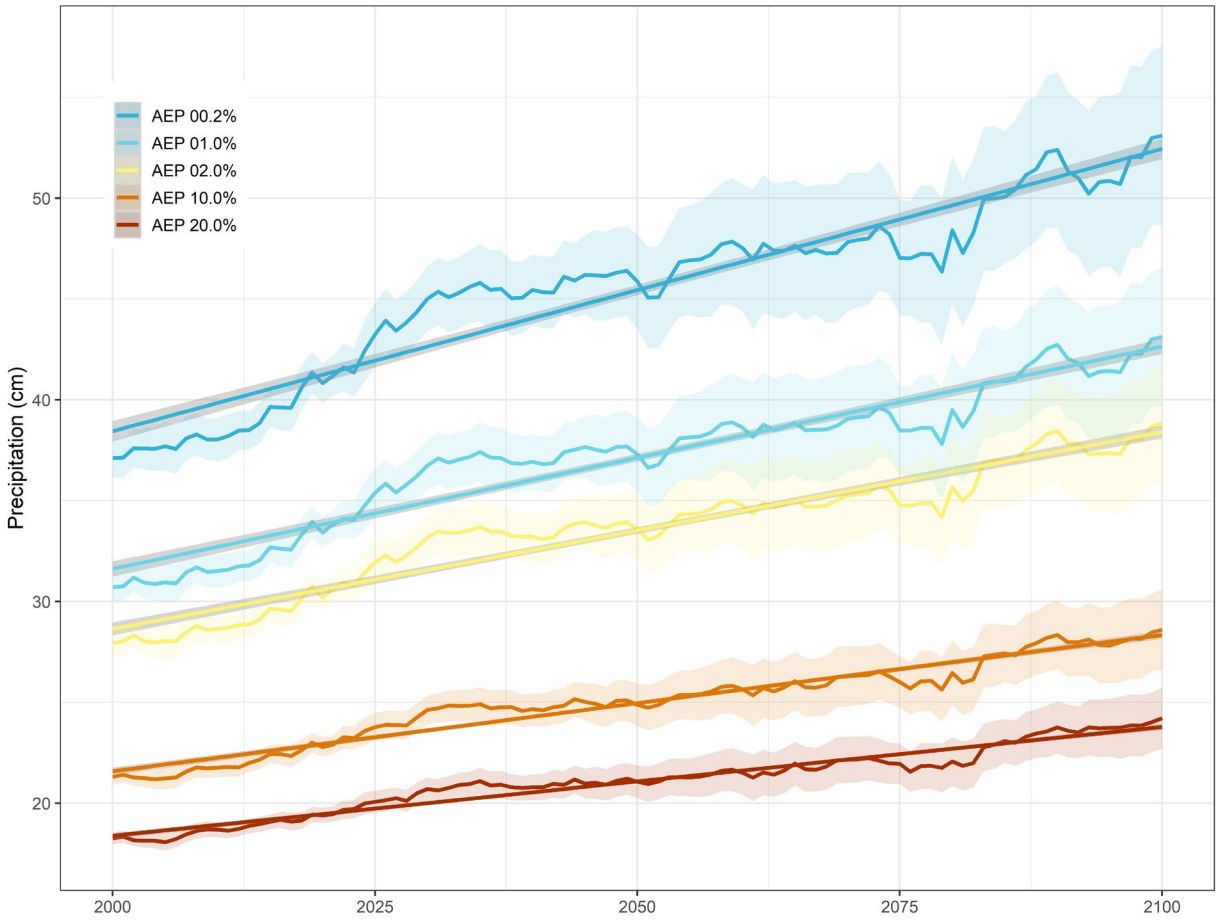

Figure 3. Precipitation volume projections. I calculate projections for the AEP 20%, AEP 10%, AEP 2%, AEP 1% and AEP 0.2% precipitation events using a Gumbel distribution with a 50-year moving window. Thick lines represent the ensemble median of 20 CMIP5 model outputs. Shaded regions represent one standard deviation of the median. Straight lines of the same color represent the linear model of each AEP precipitation event's projected rainfall volume. Under the assumption of linearity, the volume of the 20%, 10%, 2%, 1%, and 0.2% AEP precipitation events increase respectively by 0.05, 0.08, 0.10, 0.13, and 0.15 cm per year.

Expected volumes for the 24-hour AEP precipitation event are shown in Figure 3 for five AEPs: the 20%, 10%, 2%, 1%, and 0.2% precipitation events, which are based off an annual maximum precipitation volume predicted by the 20 CMIP5 model ensemble that is found in Table 7. The volume

predicted for the 20% AEP precipitation event increases from 18.3 to 24.0 cm, from 21.3 to 28.5 cm for the 10% AEP, from 28.0 to 38.7 cm for the 2% AEP, from 30.7 to 43.0 cm for the 1% AEP, and from 37.1 to 53.0 cm for the 0.2 AEP precipitation event in the Neuse River watershed over the 21st century. Additionally, the volume of the 20%, 10%, 2.0%, 1.0%, and 0.2% AEP precipitation events respectively increase by 0.05, 0.08, 0.1, 0.13, and 0.15 cm per year on average (Figure 3). Precipitation uncertainty increases for all storms over the 21st century. The relative increase in magnitude of the 0.2% AEP precipitation event exceeds more probable storms, suggesting that storm magnitude could increase inversely with a storm's statistical probability under the assumption of a Gumbel distribution. For example, Hurricane Matthew released 38-46 cm of rain over the Neuse in 2016, which Figure 3 defines as a 0.2% AEP precipitation event. However, this same rainfall volume in 2070 would be classified as a 1% AEP event, further suggesting the possibility of more severe rainfall over the 21st century. While this analysis is not able to determine changes in storm frequency, I find that the magnitude of precipitation events with a given probability increases over the century.

Land Use/Land Cover Projections

Several datasets of future LULC projections exist (Table 3). Here, land use projections are obtained from the Environmental Protection Agency (EPA) the Integrated Climate and Land Use Scenarios (ICLUS) database. I chose to use the ICLUS model because despite a coarse temporal resolution (decadal from 1970 to 2100), ICLUS offers relatively fine spatial resolution (100 m) and a variety of land use classes (18) based on the combined SSP5-8.5 scenario among other available land use models (EPA, 2017). The fine spatial resolution and number of land use classes available allow me to specify varying inputs of impervious surface and surface roughness values to the spatially distributed hydrologic model used in the coupled modeling framework for this research. ICLUS are based on modeled population growth and residential development following global Shared Socioeconomic Pathways (SSP) (i.e., socioeconomic projections) and the Representative Concentration Pathways (RCPs) (i.e., CC projections), allowing me to compliment the RCP projection determined in the climate change projections (U.S. EPA,

2017). First, I determined how each land use is predicted to change across the watershed using a chord diagram. This diagram explains the land use classification of a single 100 m by 100 m grid cell in 2020 and 2100 to observe trends in the land use transitions across the entire study area as driven by climate and socio-economic factors. Then, each land use classification is assigned a percent imperviousness and Manning's surface roughness value using the tables described in Appendix B (Exum et al., 2005; Kalyanapu et al., 2009; Zuellig et al., 2008). These datasets are input into a hydrologic model to represent spatial heterogeneities in overland storage, infiltration, and runoff routing processes.

I evaluate the change in the distribution of land use/land cover classes in the ICLUS product from 2020 to 2100 using a chord diagram (Figure 4). Chord diagrams can be used to visualize net transitions over time. In this research, such transitions represent conversion of one land use type to another. Land use is projected to vary across the watershed between 2020 and 2100 where cropland, timber, and low-density exurban are projected to transition to high-density exurban, suburban, and low-density urban uses. Most noticeably, areas classified as cropland, timber, wetland, and low-density exurban land uses are projected to decline by 845 km^2, 810 km^2, and 104 km^2, respectively, while high-density exurban, suburban (668 km^2), and low-density urban (731 km^2) land uses are projected to increase by 428 km^2, 668 km^2, and 731 km^2 (Figure 4). In contrast, there are only small increases in commercial (127 km^2), industrial (39.3km^2) and high-density urban (64.3 km^2) land uses.

The ICLUS product does not project any changes in barren land, open land, or natural waters. Wetlands are projected to decline due to increases in residential, commercial, and industrial lands. Areas classified as commercial or industrial land are projected to increase where land is currently classified as cropland, timber, or residential. While exurban growth is projected in areas currently classified as cropland and timber, exurban areas are also projected to densify into suburbs. Urban area is projected to more than double by 2100 (from 485 km^2 to 1281 km^2), mostly in exurban and suburban areas.

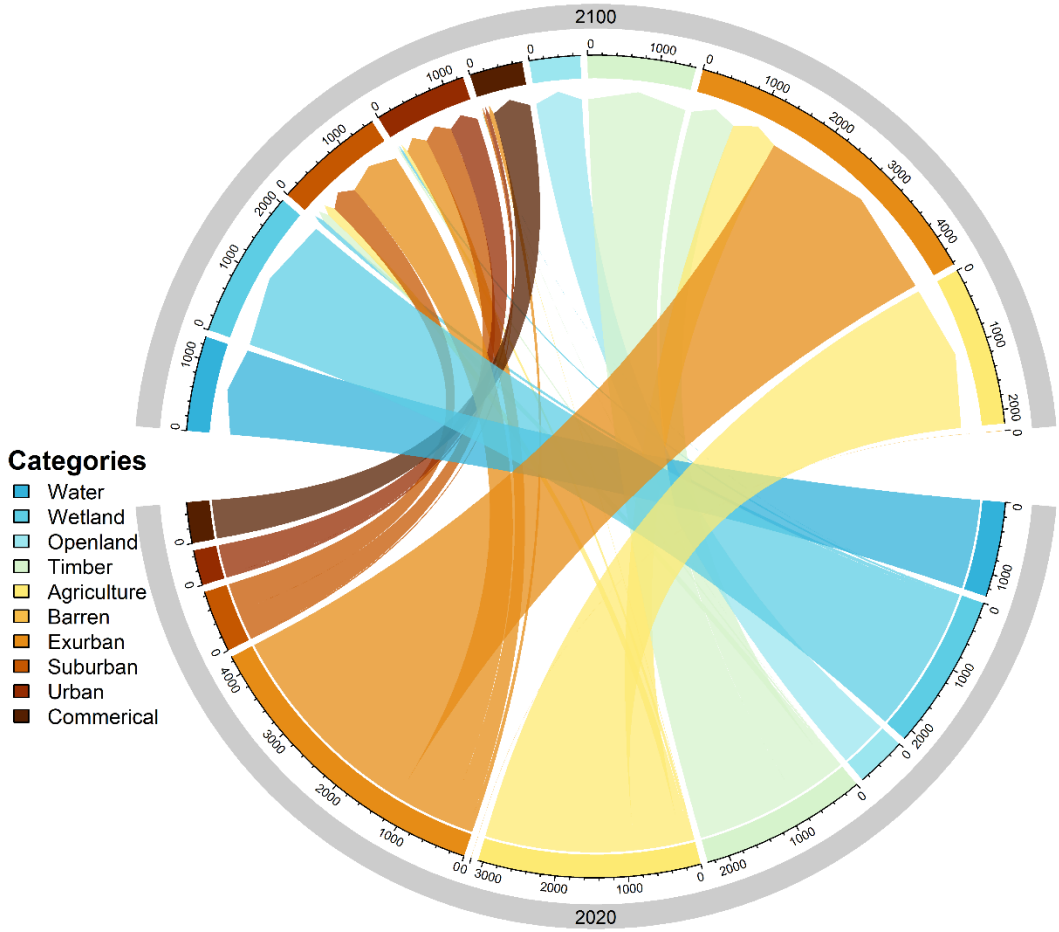

Figure 4. Chord diagram of-predicted land use change. This figure displays the magnitude of land use change in km2 from 2020 (bottom) to 2100 (top) based on the ICLUS dataset, produced with the OpenLand R package. The largest absolute change in any category is from exurban to suburban land (1194 km2); however, timber (669 km2) and agriculture lands (689 km2) will convert to exurban land at a similar rate, replacing this amount. This conversion represents an overall loss of timber and agricultural land use classes for the watershed.

These land use conversions affect the distribution of impervious surface cover and roughness, primarily seen in and around the cities of Raleigh, Wilson, Kinston, and New Bern. While these increases largely correspond to urban, suburban, and exurban growth along existing urban corridors, the ICLUS model also predicts the nucleation of dozens of new low-density urban centers in former Raleigh suburbs

as far southeast as Clayton, as far north as Durham, and as far northeast as Wake Forest, resulting in the formation of a highly impervious contiguous landscape across much of the upstream watershed. These developments reflect the recent expansion of the Research Triangle region of North Carolina, comprising the cities of Raleigh-Durham-Chapel Hill and their greater metropolitan area.

Hydrologic Model

I use Vflo® version 6.1 as the hydrologic model for this study. Vflo® is a physically based, fully distributed hydrologic model that solves the kinematic wave approximation of the shallow water equations. This simplification has been shown to describe flood wave behavior in riverine channels (Lighthill & Whitham, 1950), especially if all other terms in the full shallow water equations are insignificant (Chow et al., 1988). Vflo® solves channel and overland flow resulting from excess rainfall using a simplification of the momentum and continuity equations where R is the rainfall rate, I is the infiltration rate, h is the flow depth, and u is the overland flow velocity (Eq. 1). Here, $\partial h \,/\, \partial t$ is the change in flow depth over the change in time and $\partial(uh) \,/\, \partial x$ is the change in cross-sectional area over a change in space.

$$\frac{\partial h}{\partial t} + \frac{\partial (uh)}{\partial x} = R - I$$

Vflo® infiltrates initial precipitation using Green and Ampt parameters, which allows the model to simulate spatially distributed time-varying infiltration rates based on soils data and surface imperviousness (Rawls et al., 1983). This approach considers infiltration capacity as a function of the conservation of mass equation and shallow surficial flow that changes with time during a storm event. Excess runoff is then routed through the flow direction network using the Kinematic Wave approximation (KWA). Vflo®'s ability to accurately represent spatial heterogeneities in soil, topography, and land cover data make it a practical modeling approach for evaluating the effect of landscape and climate changes on hydrologic processes through time. Excess precipitation is then routed as overland runoff using the KWA into channel cells and subsequent discharge is represented using hydrographs. In addition to the KWA

routing method, Vflo® offers Modified Puls and Jones channel routing options to improve model calibration dependent on a variety of factors including channel storage requirements, slope, and geometry. Reservoirs also can be represented in the model using stage-storage and stage-discharge rating curves in any channel cell, enabling the inclusion of dams within the modeling framework. I refer interested parties to Vieux et al. (2004), which offers further background information and a more in-depth explanation of the model and its solver.

Vflo® takes as input digital elevation data (DEM), soil profile data, and LULCC data (Figure 5). Spatial variability in each of the input parameters is represented within the model as gridded cells across the watershed, where each cell is defined by values representing slope, hydraulic roughness, infiltration, and rainfall elevation, impervious surface fraction, hydraulic roughness, soil depth, hydraulic conductivity, wetted front, total porosity, and effective porosity (Vieux et al., 2004). I chose Vflo® because it has been widely implemented in previous hydrologic studies (Doubleday et al., 2013; Gori et al., 2019b; Juan et al., 2020; Sebastian et al., 2019) and because it efficiently solves for overland and channel flow over large domains. Additionally, Vflo®'s unique capabilities of allowing spatially distributed inputs, solving time-varying Hortonian infiltration, and enabling channel cells to be represented as reservoirs are ideal for the physical representation of LULCC, three qualities that are necessary for the success of this research.

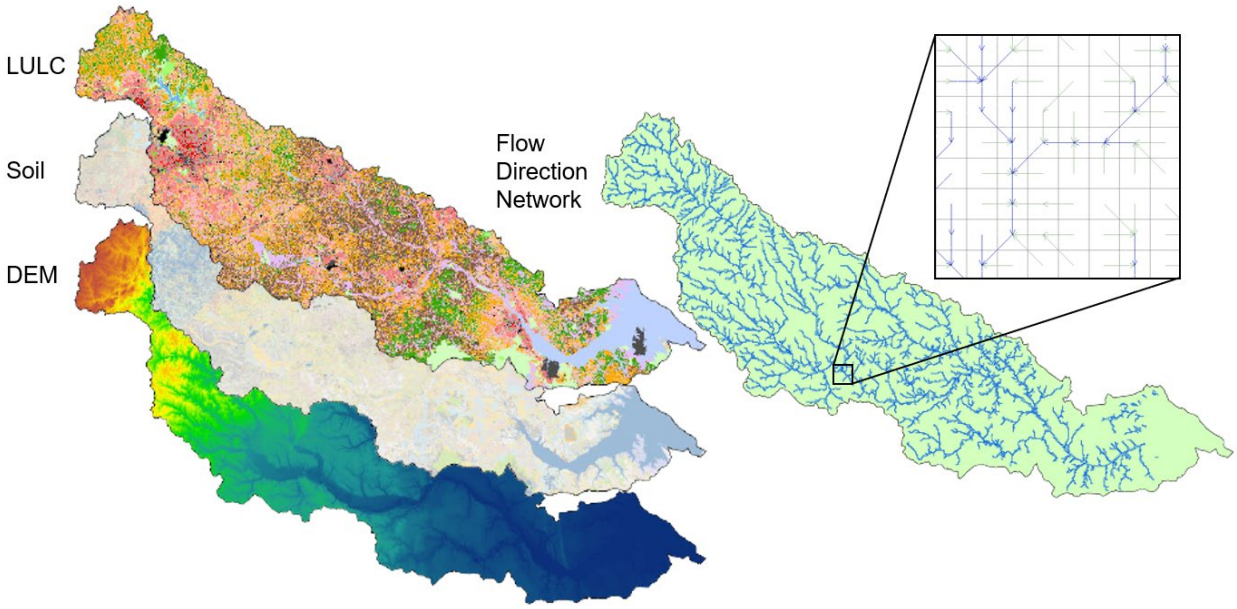

Figure 5. Distributed hydrologic model, Vflo® parameterization. A flow direction network is derived from a digital elevation model, percent imperviousness and surface roughness are derived from land use/land cover data, and infiltration parameters, including wetted front, hydraulic conductivity, depth, effective porosity, and total porosity, are derived from soils data.

Model Setup

To build the baseline model, I used Vflo® to develop a flow direction network using a 10 m digital elevation model (DEM) from the US Geological Survey (USGS) 3D Elevation Program (3DEP) National Elevation Dataset (NED). I then cut cross sections from the DEM to represent channel geometry and bathymetry to ensure that mass is conserved during flow routing. Where channel cross section data are unavailable or cannot be established, the model enforces upstream cross sections. Vflo® also allows the modeler to input stage-discharge relationships at dams and reservoir locations at downstream locations in the model to improve representation of physical processes in the model. I adjust these curves during the model calibration step, which are included in Appendix D. Rating curves were included in

Vflo® immediately upstream of all USGS stream gages in the study as well as in tributaries on the main rivers upstream of Goldsboro. The resulting model contains 123,093 cells at a 600 by 600 m resolution.

Infiltration parameters are derived using the US Department of Agriculture (USDA) Gridded Soil Survey (gSSURGO) and variable infiltration rates were predicted using the Green & Ampt equation (Rawls et al., 1983). I joined spatially distributed map unit symbols of each soil type with an associated wetted front, soil depth, effective porosity, total porosity, and hydraulic conductivity using the gSSURGO dataset in GIS to obtain distributed soils data to determine time-varying infiltration rates.

To build a baseline model representative of 2020 conditions, gridded land use/land cover data was obtained from the Multi-Resolution Land Characteristics (MLRC) National Land Cover Database (NLCD) for 2016 at a 30-m resolution. LULC was reclassified in terms of its percent imperviousness and Manning's roughness based on values provided by Exum et al. (2005) and Zuellig et al. (2008) (imperviousness) and Kalyanapu et al. (2009) (roughness). These attributions enable Vflo® to represent the physical effect that different land cover classifications have on hydrologic processes including infiltration and overland flow. I determine channel roughness to be 0.035 across the domain, since this value consistent with a clean, straight, full stage natural stream with a flood stage width of 33 m and a floodplain consisting of high grass or mature row crops as defined by Chow (1988).

Finally, the model assumes that precipitation predicted by the ensemble of CMIP5 climate models is distributed in time using an SCS Type II intensity-duration-frequency (IDF) curve (USDA, 1986). An IDF curve relates a given rainfall intensity with an associated duration and frequency. The SCS Type I curve represents the wet winters and dry summers of the US Pacific Coast, the SCS Type II curve characterizes the climate of the interior US, and the SCS Type III curve embodies the heavy rainfall produced by tropical storms and hurricanes along the US Atlantic and Gulf Coasts (Feldman, 2000). I chose the SCS Type II curve for this research since the Neuse is primarily inland and is only coastal along at the watershed's downstream end.

Model Calibration/Validation

I obtain gauge-adjusted radar rainfall data from NOAA's National Severe Storm Laboratory (NSSL) Multi-Radar/Multi-Sensor System (MRMS) stored in the Iowa State Repository to calibrate the baseline model. When assessing relevant storms for calibration, I favor precipitation events exceeding a 1% annual exceedance probability (AEP) and that occurred temporally after the modeled surface characteristics are reported (i.e. after 2016). These selection criteria are important since the model is built to represent large storm magnitudes well across a landscape that reflects current land uses. These storms include Hurricanes Matthew (2016), Florence (2018), and Dorian (2019). I calibrate the model against Hurricane Matthew due to the storm's relatively symmetrical hyetograph and large magnitude. I then validate the model against six additional storms to ensure a robust hydrologic model.

Table 1. Calibration event details.

Event	**Formed**	**Dissipated**	**Damages (2016 USD)**	**Deaths**	**Maximum Wind (km/h)**	**Total Rain near Goldsboro (cm)**
Bonnie	2016-05-27	2016-06-09	640,000	2	75	NA
Unnamed	2017-04-23	2017-04-25	NA	NA	NA	NA
Unnamed	2017-05-04	2017-05-05	NA	NA	NA	NA
Matthew	2016-09-28	2016-10-10	16,470,000,000	603	270	39.3[1]
Florence	2018-08-31	2018-09-18	24,230,000,000	54	240	36.6[2]
Michael	2018-10-07	2018-10-16	25,500,000,000	74	260	0.6[3]
Unnamed	2018-11-12	2018-11-13	NA	NA	NA	NA
Dorian	2019-08-24	2019-09-10	5,100,000,000	329	295	11.8[4]
Isaias	2020-07-30	2020-08-05	4,730,000,000	17	150	8.6[5]

[1]Stewart (2017); [2]Stewart & Berg (2019); [3]Beven et al. (2019); [4]NWS (2019); [5]Latto et al. (2021)

I use the dataRetrieval tool developed by the USGS in R (DeCicco, 2021) to access discharge and stage observations at nine USGS stream gages. I evaluate model performance using the Nash-Sutcliffe Efficiency (NSE), Root Mean Squared Error (RMSE), and Pearson Correlation Coefficient. NSE reports the variance between a modeled hydrograph and an observed time-series, where a perfect model has an NSE of 1 (Mccuen et al., 2006). RMSE is the standard deviation of the residuals, which predicts how concentrated modeled data is around a line of best fit for the observed data (Chai & Draxler, 2014). Since RSME reports the variance of measured and modeled data, values of RSME can be large, and so smaller RSME values represent a better model. The Pearson Correlation Coefficient is a measure of linear correlation between two sets of data. Thus, it is a normalized measurement of the covariance where a perfect model has a value of 1 while a perfectly incorrect model has a value of -1. Peak discharge, volume, and timing can be exported for determination of differences between simulated and observed values (Table 2).

Table 2. Model calibration and validation statistics.

USGS ID	**Name**	**Hurricane Matthew (Calibration)**			**Hurricane Florence (Validation)**		
		RMSE	**NSE**	**Pearson**	**RMSE**	**NSE**	**Pearson**
02088000	Middle Creek nr Clayton	1805.35	0.96	0.98	390.91	-0.41	0.77
02087275	Crabtree Creek at HWY 70	664.31	0.67	0.90	406.18	0.45	0.93
02087500	Neuse River nr Clayton	1470.96	0.92	0.96	2681.61	-1.42	0.40
02089000	Neuse River nr Goldsboro	11868.76	0.41	0.69	4131.87	0.78	0.90

02089500	Neuse River nr Kinston	10356.35	0.15	0.62	4581.29	0.73	0.89
02091500	Contentnea Creek at Hookerton	6125.21	0.44	0.78	1600.63	0.76	0.89
0208758850	Swift Creek nr McCullars Crossroads	200.11	0.96	0.98	198.06	-0.69	0.92

The uncalibrated model routes water too efficiently through the watershed, on the order of 3-4 days. This is likely due either to the watershed's relatively low gradient and wide floodplain, which enables greater storage capacity and slower conveyance during large storm events, or a problem with the Kinematic Wave approximation, which does not conserve momentum during hydrologic routing. I first reduce this error by increasing surface and overland Manning's n (roughness) values to improve the routing in the model. This approach leads to greater errors and physically misrepresents the effect of current land cover. I then attempt to reduce error by increasing the storage capacity of the channel at select locations by determining stage-storage and stage-discharge relationships for USGS gages and the actively managed Falls Dam reservoir east of Raleigh (USACE, 2013). I include additional rating curves for locations along the main channel and tributaries from a USACE preliminary HEC-HMS model that were developed for a hindcast analysis of Hurricane Florence to further improve calibration (Yi, 2021).

I validate the model against hydrographs representing Hurricane Florence (Table 2). High RMSE values for the Hurricane Matthew calibration are likely due to the complexity of releases from the actively managed Falls Dam reservoir, which was closed during Matthew's initial precipitation but opened as downstream hydrographs continued to peak. Conversely, downstream river stages during Hurricane Florence required a prolonged dam closure, thus resulting in a multipeak hydrograph behavior with a dominant first peak (USACE, 2018). The calibrated model resulted in high Pearson values for Hurricane Florence despite poor NSE values at gages 02088000, 02087500, and 0208758850. The active

management of an upstream reservoir limits the effectiveness of the passive hydrologic model relying on single rating curves at locations across the domain. As such, my analysis assumes there is a predetermined dam operation procedure represented by the stage-discharge relationships. This approach is an improvement for calibration and validation; however, it fails to represent small deviations from operation by predictably releases water as a function of reservoir level as opposed to downstream flooding.

Figure 6 shows that the calibrated model performance improves upon the uncalibrated model in predicting measured discharge peaks for nine storms at seven USGS gage locations. I first compute a non-parametric paired-sample Wilcoxon test to determine whether the calibrated and uncalibrated model results are statistically different from each other. From this test, I conclude that the median discharge of the uncalibrated model is significantly different from the median discharge after calibration because the p-value = 6.5e-09 is less than the significance level alpha = 0.05. Since the datasets are statistically different, I can now consider how the modeled and measured data compare to a 1:1 line. The Wald test tests if a slope differs significantly from a line with a slope of 1.

$$W = \frac{(\hat{\beta} - \beta_0)}{se(\hat{\beta})} \approx N(0,1)$$

Where β_0 = 1 to test whether the slope is different than 1. Note also that a p-value approaching 0 is evidence that the slope is different than 1. The Wald test finds that the uncalibrated model has a p-value of 0.003 and the calibrated model has a p-value of 0.065. This provides the first evidence suggesting that the uncalibrated model slope is less like 1 than the calibrated model. I calculate the confidence interval for the coefficient of a linear model between measured and modeled discharge peaks. If the 95% confidence interval doesn't include 1, then the slope is significantly different from 1. At a 95% confidence interval, the uncalibrated model slope is 2.68 and the calibrated model slope is 1.01. Therefore, I reach the same conclusion as the Wald test that the slope of the uncalibrated model is statistically different than 1 but the slope of the calibrated model is not statistically different than 1 at a 95% confidence interval.

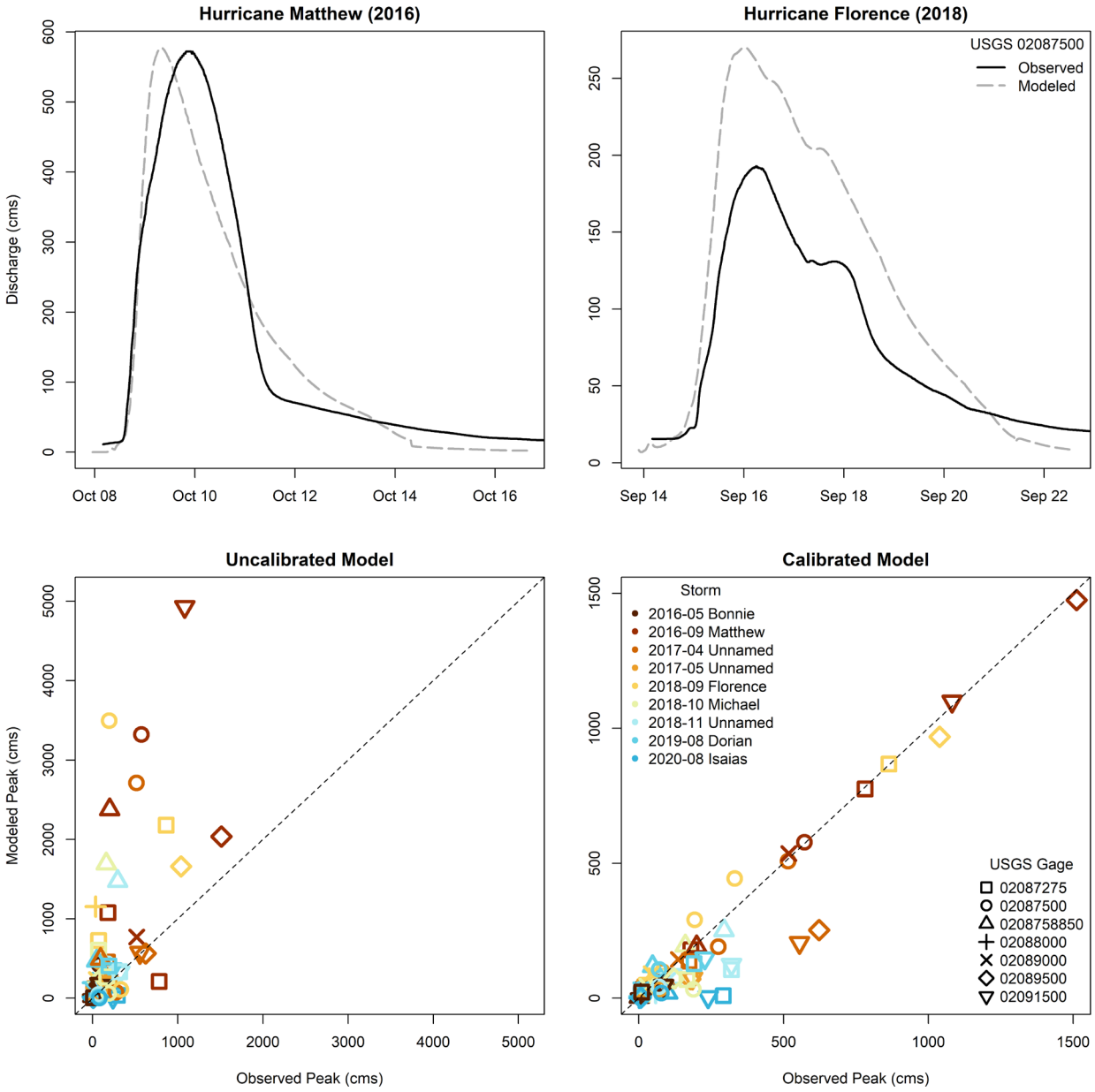

Figure 6. Hydrologic model calibration and validation. Figures 6a and 6b describe hydrographs of discharge after calibration for Hurricanes Matthew and Florence at USGS 02087500. Figures 6c and 6d represent model performance before and after hydrologic calibration for 9 storm events at 7 USGS gages. The calibrated model performs significantly better than the uncalibrated model at predicting measured discharge peak from 2016 to 2020. At a 95% confidence interval, the uncalibrated model overpredicts peak discharge by 2.68 times whereas the calibrated model overpredicts peaks by 1.01 times.

Hydraulic Model

The Hydrologic Engineering Center – River Analysis System (HEC-RAS) is a system of software designed to model water surface profiles (USACE, 2016). HEC-RAS enables a river's physical representation as geometric approximations of reaches, tributaries, banks, and cross-sections. While some data can be manually input such as cross-sectional data at river stations, terrain data derived from a DEM can further assist model development. Then, at a subset of river stations, the user can enter either continuous hydrographs or peak discharge rates for unsteady flow and steady flow simulations respectively. HEC-RAS outputs include a raster of inundation depths as well as a vector of inundation extent across the domain. For this assessment, a steady flow simulation is run to generate a conservative estimate of future floodplain depth and extent under each future scenario.

Results

I report how spatial and temporal trends in LULCC and climate-induced changes in precipitation intensity for five events with varying statistical return periods (pertaining to annual exceedance probabilities (AEP) ranging from 20% to 0.2%) may influence future peak discharges across the watershed. Then, I determine how projected changes in peak discharge would affect flood hazard and exposure across three tributaries for a case study in Goldsboro, NC.

Hydrologic Modeling in Neuse River Watershed

The percent increase in peak discharge relative to a 2020 baseline scenario are shown in Figure 7 at the downstream outlet of each HUC 10 sub-watershed (n = 39). In 2020, the 1% AEP precipitation event is predicted to be 30.7 cm/24 hr (Table 7), generating a peak discharge of 1,076 cms in Goldsboro and 821 cms in Kinston. When isolating the effects of climate in the LULCC scenario, I find that peak discharge remains within 20% of baseline conditions by 2100, ranging between a small decrease of 1.5% to an increase of 17.7% (Figure 7a). Only one HUC 10 is projected to have a decline in peak discharge, despite the sub-watershed experiencing an increase in exurban low- and high-density areas. When

controlling for the effects of LULCC, I find that the same 1% AEP precipitation event in 2100 is predicted to release 43.0 cm of water, a 29% volume increase over the 2020 value. The effect of this increase results in an increase in peak-discharge between 36.9 and 79.4% across the watershed. Furthermore, the impact of both scenarios results in a peak discharge increase between 42.0 and 88.2%.

Figure 7 also illustrates discharge trends across the Neuse River basin. In the LULCC scenario, the greatest relative increases in peak discharge occur immediately downstream of urbanizing regions around Wake Forest (17.7%), Kinston (16.0%), Wilson (13.5%), and New Bern (13.5%) as well as downstream of southeastern Raleigh through Clayton (Figure 7). This finding suggests that the role of LULCC on controlling increases in discharge peak becomes relatively more important as the upstream contributing area decreases. Outside of these regions, impervious surfaces are less concentrated, which correlates with marginal increases in peak discharge over the 21st century. The CC scenario predicts spatially uniform increases in rainfall, leading the greatest relative increases further downstream in Kinston (79.4%), Goldsboro (74.4%), and Smithfield (67.3%). Similarly, the combined scenario reflects both general downstream increases as well as greater peaks adjacent to projected urbanizing regions. This includes upstream of Goldsboro along the Little River (88.2%), Kinston (83.8%), and near New Bern (83.2%).

The watershed does not respond linearly to the combined scenario that considers the joint impacts of climate change and land use/land cover changes. Instead, a positive, non-linear feedback, that exceeds the additive effect of each independent scenario on peak discharge trends is observed (Figure 8). I calculate this change by 2100 as the difference between the percent change in peak discharge predicted under the combined CC + LULCC scenario and the sum of the percent change predicted under each of the individual CC and LULCC scenarios. Figure 8 shows that peak discharge increases disproportionately more in the CC + LULCC scenario than in both the CC and LULCC scenarios when added together. A positive value line indicates that discharge predicted by the combined scenario exceeds the sum of the independent scenarios and a negative value suggests that the combined scenario is less than the sum of the independent scenarios. Furthermore, since the vertical distance from the horizontal line indicates the

magnitude of difference, smaller contributing areas demonstrate a stronger multiplier effect than larger areas. The majority of the 39 sub-watersheds are clustered in the positive graphical space, and are clumped among sub-watersheds with smaller contributing areas. This 'washing out' effect further suggests that this non-linear influence has proportionally more influence on amplifying discharge peaks locally where heterogeneous land use changes spatially connect more impervious and less rough land cover. While a few HUC 10's plot along the zero line, and a few more indicate a weak negative non-linear response to the combined scenario, the sub-watershed that coincides with Kinston, NC exhibits a strong negative non-linear response (-11.7%).

When comparing hydrographs between 2020 and 2100 for the five AEP precipitation events, changes in time to peak are greatest for the AEP 10% and changes in peak discharge are greatest for the AEP 0.2% precipitation events relative to the other AEP precipitation events (Figure 9). While Figure 7 only reports changes between 2020 and 2100 for the 1% AEP precipitation event and is intended to illustrate discharge trends that result from each scenario, Figure 9 describes changes for all five AEP precipitation events at a single location: USGS 02089000 near Goldsboro, NC. Both figures indicate that discharge increases more for lower probability events. Figure 9b further shows that the 2100 CC + LULCC scenario decreases time to peak by 1.6 hours (AEP 20%), 8.1 hours (AEP 10%), 6.7 hours (AEP 2%), 4.6 hours (AEP 1%), and 3.2 hours (AEP 0.2%) relative to the 2020 baseline. The 2100 scenario also increases peak discharge by 329 cms AEP 20%), 577 cms (AEP 10%), 1,448 cms (AEP 2%), 1,713 cms (AEP 1%), and 2,331 cms (AEP 0.2%) over 2020 projections.

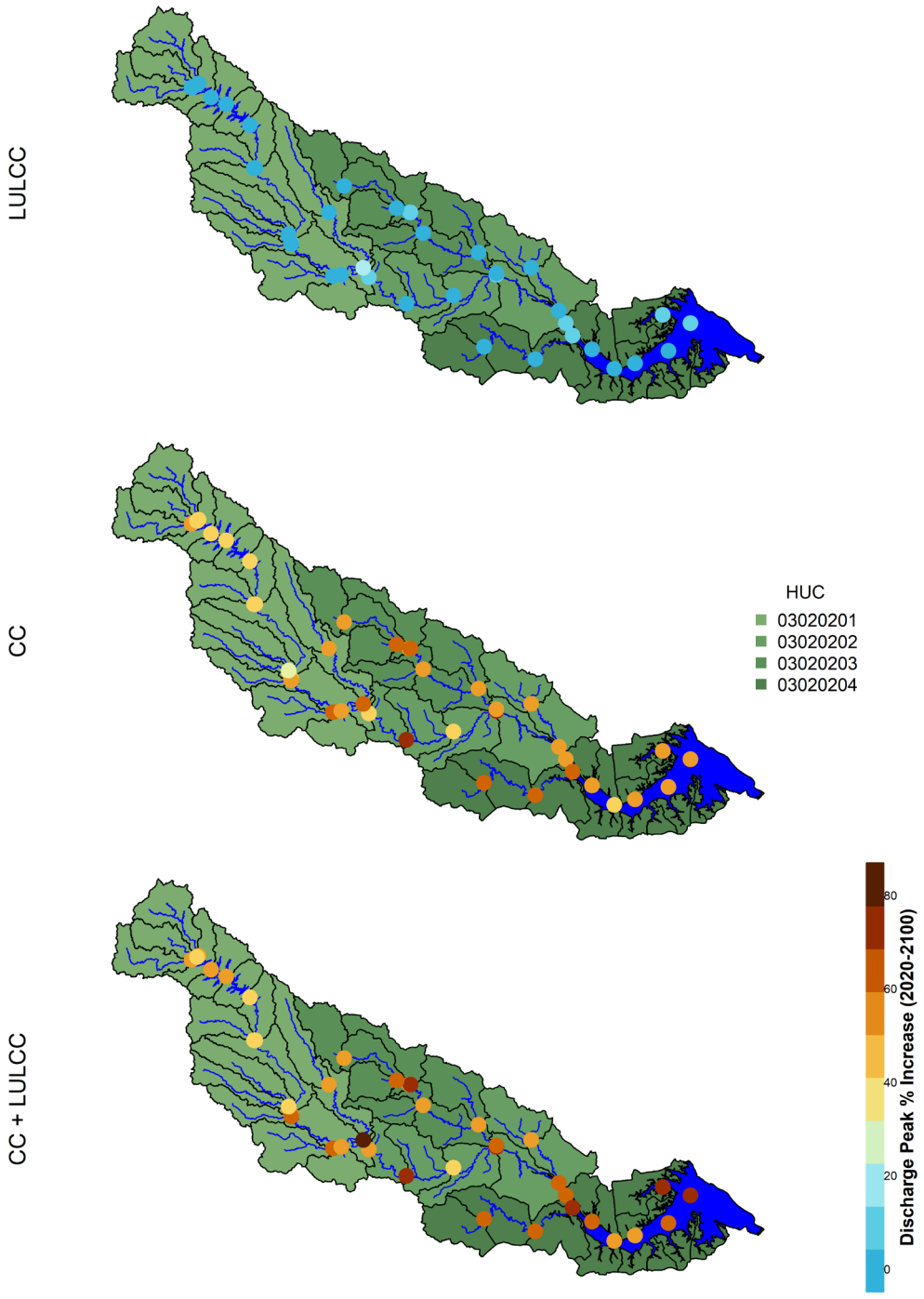

Figure 7. Watershed peak discharge increases. Figure 7a represents the land use/land cover change scenario, Figure 7b indicates the climate change scenario, and Figure 7c illustrates the combined scenario. The climate change scenario reflects the increase peak discharge due to the 1% AEP precipitation event. Four HUC 8's are represented as varying shades of green, and 39 HUC 10's are represented by black

borders. Peak discharge increases the most in HUC 0302020116 in the LULCC (17.7%) and CC + LULCC (88.2%) scenario. This HUC is on the Little River upstream of Goldsboro, which experiences a conversion of primarily cropland to primarily low and high density suburban and urban land use around a town within the HUC boundary.

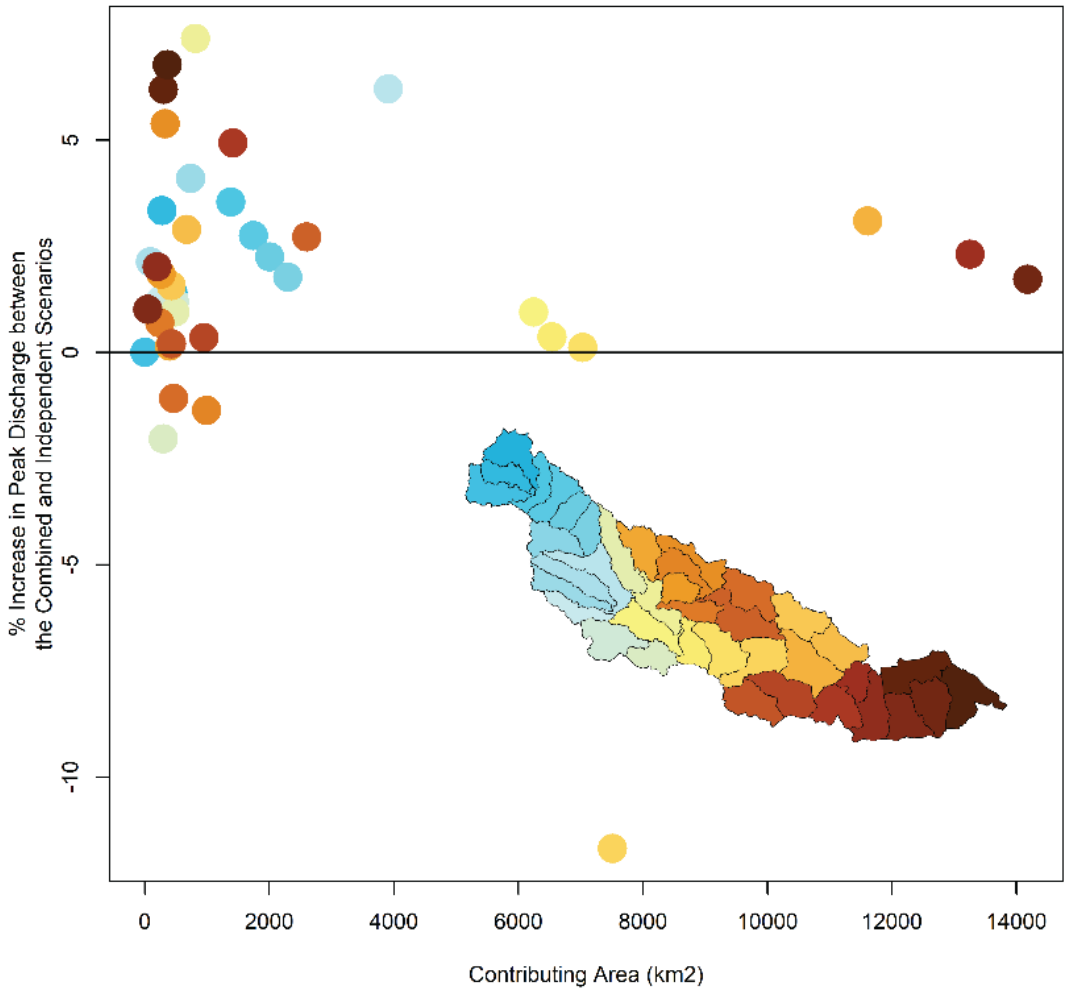

Figure 8. Non-linear differences in peak discharge between scenarios. Percent difference between the increase in peak discharge predicted by the combined scenario and by the linear addition of the peak discharge increases derived from the two independent scenarios at the outlet of each HUC 10 sub-watershed in the Neuse River basin. Positive values indicate a positive, non-linear effect of the combined scenario; points along the zero line indicate that there is a near--linear relationship between the

independent scenarios and the combined scenario; negative values indicate a negative, non-linear effect on peak-discharge. The color of the point corresponds to the location of the sub-watershed as indicated on the map in the bottom right. Most locations display a non-linear trend.

Figure 10 continues this assessment by quantifying decadal trends across scenarios and different probabilistic storms. The LULCC-only scenario predicts linear increases in peak discharge and increases by a median value of 4.2% per decade over the 21st century. This is likely due to a constant rate of land use conversion events from primarily timber and agricultural land uses to exurban, suburban, and urban land uses predicted by ICLUS, which reduces the watershed's capacity for flood retention at an almost constant rate. Conversely, the CC-only scenario projects that peak discharge will increase non-linearly by 2100. Disparities in the relative increase in peak discharge become apparent in this scenario: the frequent 20% AEP precipitation event median peak discharge increases less by 2100 than for less frequent storms. The median storm volume of the 0.2% AEP increases the most by 2100 (54.6%) relative to the 20% AEP precipitation event (48.2%). However, the combined scenario yields the greatest increases across all storms relative to the independent scenarios, ranging from 55.4% for the 20% AEP precipitation event and 59.3% for the 0.2% AEP precipitation event in 2100 relative to 2020 peaks (Figure 10). The combined scenario reflects many of the trends observed in the individual climate change and land use land cover change only scenarios. Climate plays a more dominant role in controlling the trend in discharge peak across the entire watershed (as shown in Figures 8 and 10). Furthermore, it is possible to consider the role that contributing area plays on affecting discharge peak when assessing the non-linear effects of the combined scenario on hydrology over just the addition of the two independent scenarios.

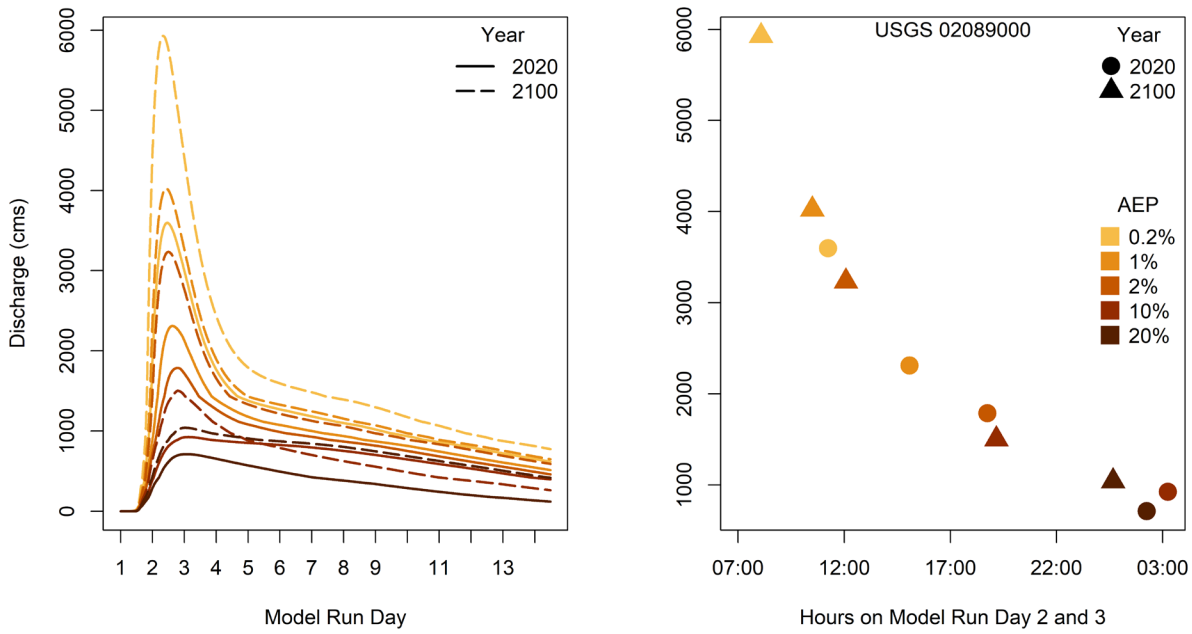

Figure 9. Change in hydrograph peak discharge and timing relative to a 2020 baseline condition. Figure 9a reports the hydrograph for each AEP precipitation event over a two-week model run while Figure 9b represents changes in the time to peak for each hydrograph plotted in Figure 9a. There is an exponential relationship between peak discharge and timing for the five AEP precipitation events across the two time periods plotted.

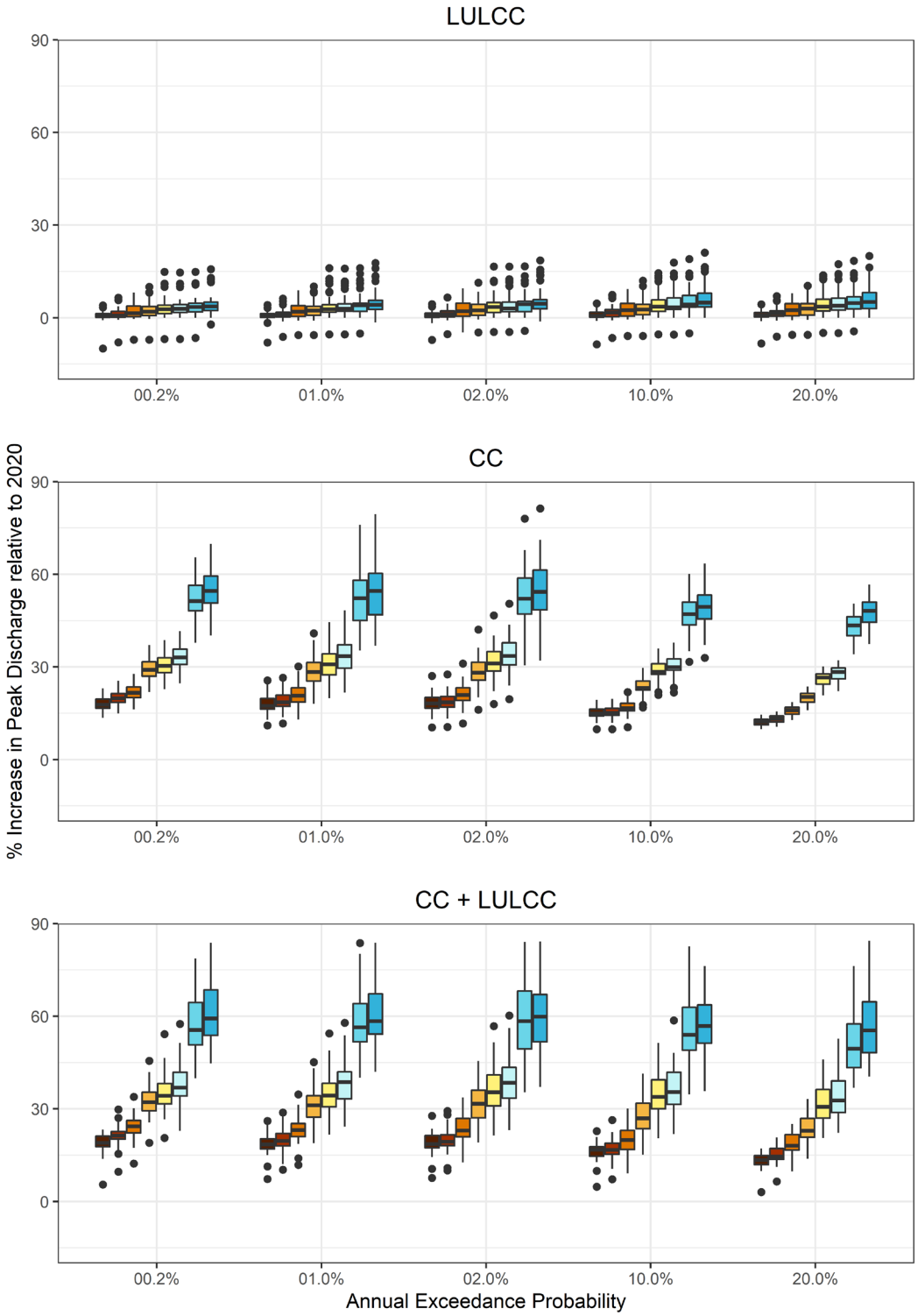

Figure 10. Change in boxplot peak discharge relative to a 2020 baseline condition. Figure 10a illustrates the land use/land cover change scenario, Figure 10b represents the climate change scenario, and Figure 10c is the combined scenario. Each set of boxplots demonstrate relative increases for five probabilistic

storm events. The 0.2% AEP precipitation event under the CC + LULCC scenario has the greatest increase in peak discharge (54.6%) in 2100 relative to 2020.

Floodplain Analysis for Goldsboro, NC

Three tributaries to the Neuse River run through Goldsboro, NC. Floodplains are shown in Figure 11 for five AEP precipitation events in 2020 (a) and 2100 (b). Changes in inundated area vary across three tributaries: Little River (west Goldsboro), Big Ditch (central Goldsboro), and Stoney Creek (east Goldsboro). While the Little River floodplain is by far the largest within city limits (373 km^2), there are relatively few buildings located within Little River's current or future floodplain extent. Changes in the Little River floodplain are primarily northwest of Goldsboro city limits, a largely rural, uninhabited area. In contrast, Big Ditch has a relatively small contributing area (12 km^2 relative to Little River's 816 km^2 and Stoney Creek's 74 km^2), yet the Big Ditch floodplain and floodplain fringe are particularly developed as they bisect the center of Goldsboro and flow for 5 km before exiting into the Neuse.

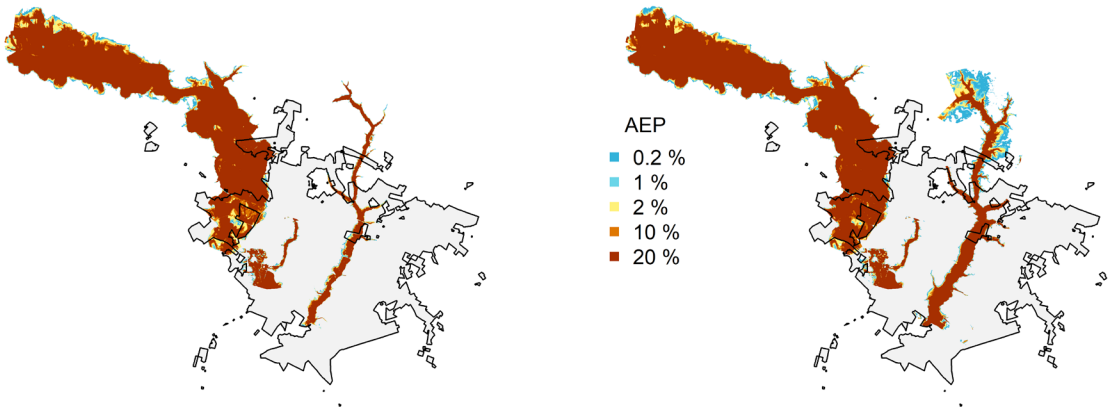

Figure 11. Modeled floodplain extent in Goldsboro, NC. The city boundary is defined by the black outline and each probabilistic floodplain extent is shown using the blue-red color spectrum. The dark red color represents the 20% AEP floodplain, and the blue represents the 0.2% AEP floodplain. The 20% AEP floodplain increases by 6 km^2 between 2020 and 2100 across the three tributaries.

Figures 11 and 12 illustrate the extent and depth of the floodplain for three Goldsboro tributaries. The increase in floodplain area is relatively large, with the 20% AEP flood extent increasing by 8 km^2 with respect to 2020 and the 0.2% AEP extent expanding by 9.2 km^2 under the combined scenario (Figure 11). The spatial variability in flood depth in 2020 (a) and 2100 (b), and the difference in depth (c) for five probabilistic storms is plotted in Figure 11. The results demonstrate that the greatest relative changes in water depth occur along Stoney Creek. These relative changes increase in the upper reaches of the Creek as AEP precipitation event volume increases. For example, water depth in the upstream tributaries to Stoney Creek increases by 3.6 m between 2020 and 2100 under the 20% AEP precipitation event, but by 5.0 meters under the 0.2% AEP precipitation event.

When flood hazard area is plotted against building locations, changes in exposure along the Stoney Creek tributary are disproportionately greater than in Little River or Big Ditch under all future scenarios (Figure 13). Focusing on the 0.2% AEP precipitation event (Figure 13, row 5), Stoney Creek hazard area increases by 72.4% (LULCC), 59.0% (CC) and 179% (CC + LULCC) which results in an increase in exposure by 331.8%, 271.0%, and 700% respectively. This appears primarily due to variability in the extent of Stoney Creek, which has a low-angle right bank that provides a greater channel capacity which encroaches on eastern Goldsboro. While each independent scenario had varying degrees of influence on discharge peaks at the watershed scale (Figure 7), it appears that future predicted LULCC plays as important a role in the relative increase in flood hazard extent and exposure as CC since each of the leftmost two columns report similar findings for all probabilistic storms.

This finding would further support the interpretation of Figure 7, which showed that the LULCC-only scenario poses greater control on hydrologic processes than the CC-only scenario where heterogeneous increases in impervious surface and decreases in surface roughness connect to form impervious patches across the watershed (Appendix C). The combined scenario (Figure 11c) demonstrates that LULCC and CC generate positive, non-linear effects on flood hazard extent.

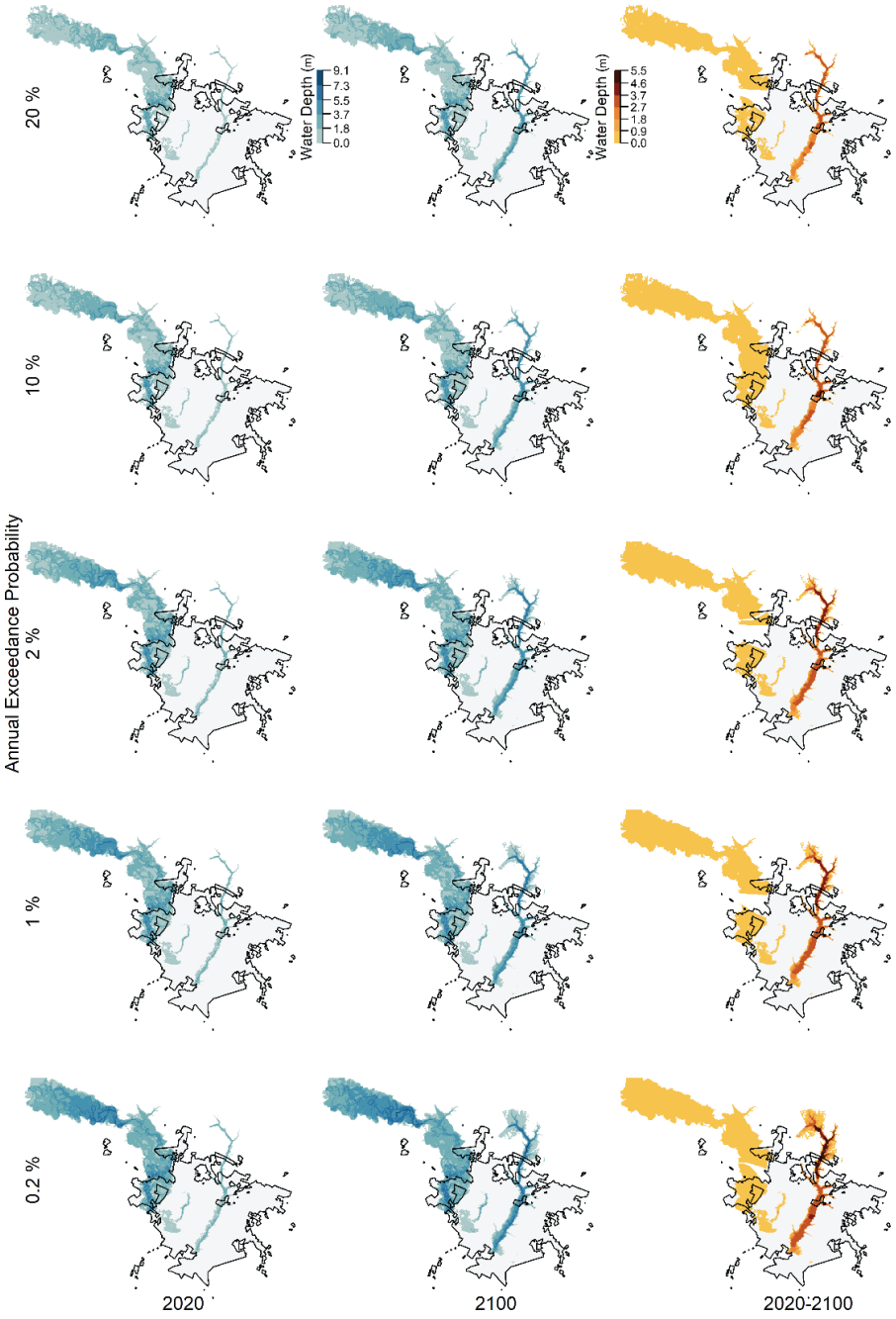

Figure 12. Modeled water depth (m) in Goldsboro, NC. Flood hazards in 2020 and 2100 (blue), and the increase in flood depth between 2020 and 2100 (orange) for each AEP precipitation events. Water depths increase by: 3.64 m (20% AEP); 4.17 m (10% AEP); 4.28 m (2% AEP); 4.51 m (1.0% AEP); and 5.00 m (0.2% AEP).

Where the independent projections yield increases in flood hazard extent of 3, 9, and 80% (LULCC: Little River, Big Ditch, Stoney Creek) and 2, 6, and 70% (CC: Little River, Big Ditch, Stoney Creek), the combined scenario results in a 6, 13, and 117% (Little River, Big Ditch, Stoney Creek) increase for the 20% AEP precipitation event in 2100. This suggests that the combined scenario only exceeds the sum of the independent scenarios in the Little River tributary. These results contrast with the 0.2% AEP precipitation event, which in 2100 predicts hazard extent increases of 0.6, 9.1, and 72.4% (LULCC: Little River, Big Ditch, Stoney Creek), 2, 9, and 59% (CC: Little River, Big Ditch, Stoney Creek), and 2, 16, and 179% (CC + LULCC: Little River, Big Ditch, Stoney Creek). In this event, the combined scenario exceeds the sum of the independent scenarios in the Stoney Creek tributary. This suggests that each scenario exerts control of a similar magnitude on hydrologic processes for this low-gradient, Piedmont to Coastal Plain watershed setting, both at the watershed scale and locally in a manner proportional to the degree of heterogeneous land use changes.

The exposure to the current building stock for each flood hazard scenario is also shown in Figure 13. Exposure increases proportionally to hazard extent in Little River and Big Ditch when isolating either climate change or land use/land cover change. Flood exposure increases more along Big Ditch (520 to 581 buildings) in response to LULCC than to CC (520 to 562) under the 0.2% AEP precipitation event. However, the opposite is true along Little River, which experiences an increase from 608 to 624 buildings when isolating LULCC and from 608 to 671 buildings when isolating CC. This provides further evidence that contributing area influences the magnitude of impact that LULCC has on peak discharge and subsequent flood hazards. Stoney Creek also displays this contribution area effect on LULCC influences (148 to 639 buildings) relative to CC influences (148 to 549 buildings). Under the combined scenario and a 0.2% AEP precipitation event, 2,421 buildings are predicted to be exposed. The amplifying effect of the combined scenario further exacerbates exposure in Stoney Creek; the number of exposed buildings in the combined scenario (1184) is more than then number of exposed buildings when isolating for CC (549) and LULCC (639) separately.

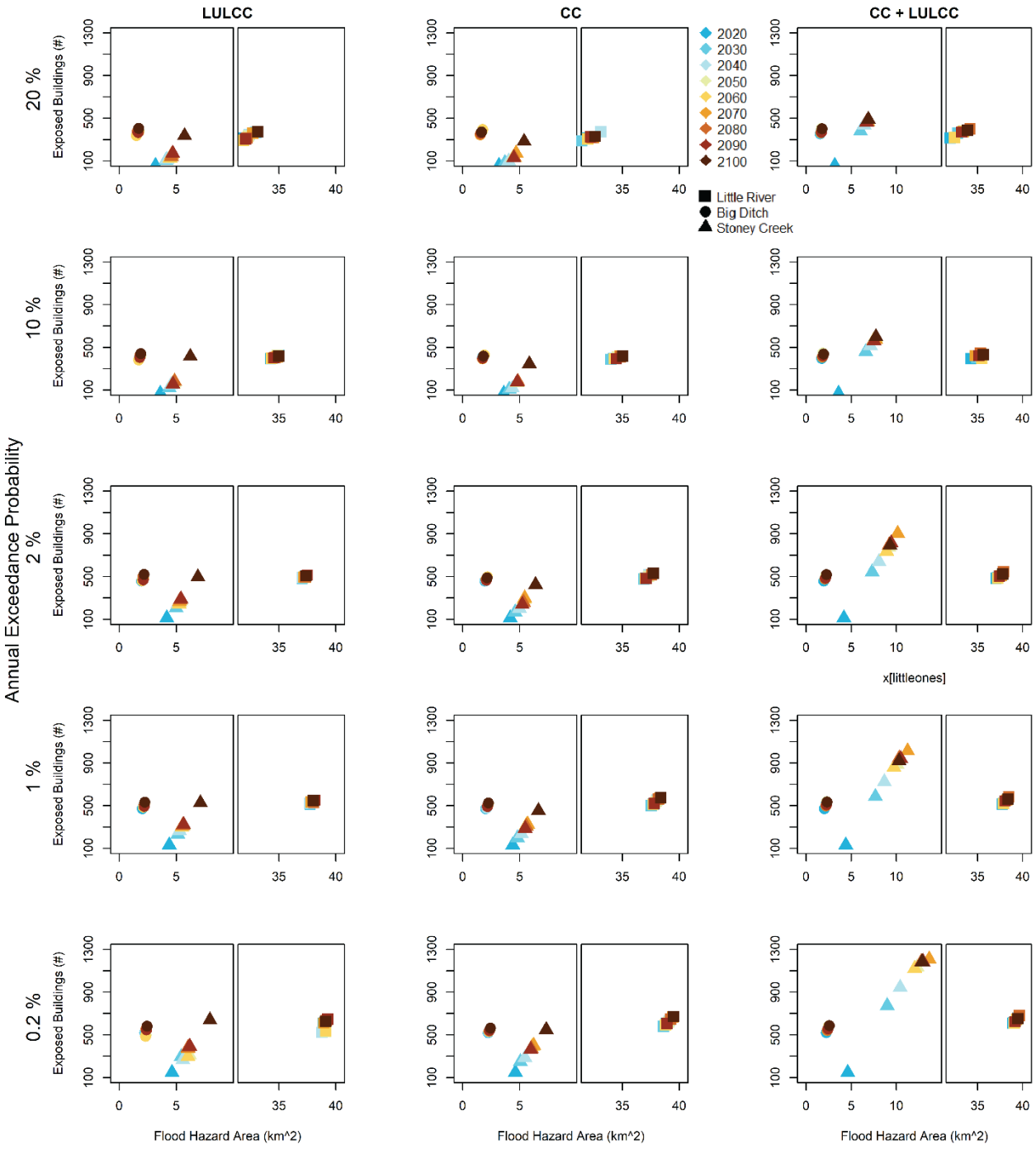

Figure 13. Flood hazard extent and exposure in Goldsboro, NC. Each tributary is represented by shape and years are represented by color. Results are stacked by scenario (columns) and probabilistic storm intensity (rows). In Stoney Creek, flood hazard extent increased by 2.8 times and flood exposure increased eightfold under the 0.2% AEP CC + LULCC scenario.

Discussion

Key Results

Since floodplains serve as the primary marker of risk in the US and influence policies concerning development, risk reduction, recovery, and mitigation, this thesis aims to understand the role of future LULC and CC on floodplain expansion. This is especially important coastal plain areas, where most of the world's human population lives and where large increases in flood risk are apparent as represented by increasing flood losses. In this thesis, I use the Neuse River Watershed in Eastern North Carolina to explore how future projections will influence floodplain hydrology, focusing on the City of Goldsboro to analyze what impact these changes will have on floodplain extent. This study considers the role that an ensemble of twenty GCM's (CMIP5) and one land use model (ICLUS) have in predicting increases in future discharge and flood hazards across a primarily rural, coastal, low-lying watershed.

I found a predominant climatic control on future discharge. I also observe a spatial decoupling between increases in design storm volume in the upstream regions and increases in discharge peak downstream. Peak discharge increases by 5% under the land use scenario, 55% under the climate scenario, and 62% under the combined scenario. The combined effects of climate and land cover are propagative, producing non-linear increases in runoff that exceed the contribution of each driver's runoff individually. This has been observed previously in SE US watersheds (Huq & Abdul-Aziz, 2021; Lafontaine et al., 2015; Suttles et al., 2018), further underscoring the importance for research to quantify the controlling factors of discharge propagation so that projected flood hazards incorporate relevant processes into hazard analyses.

Results suggest that peak discharge will increase at locations more immediately downstream of concentrated urbanizing regions in the land use land cover change scenario as well as proportionally more in the middle and lower Neuse watershed in the climate change scenario (Figure 10b). The disproportionate role that climate plays in the combined analysis underscores the watershed's primarily agricultural characteristics, which reflect permeable surfaces and characteristically high surface

roughness. This result adds support to similar studies (Table C.5) that generally find that peak discharge is influenced more by climate change than by land use-land cover change. For example, discharge peaks increased under land use change by 54%, climate change by 20%, and the combined scenario by 84% in the highly urbanized Buffalo-San Jacinto watershed (2,531 km^2) in the Houston, TX region (Sebastian et al., 2019). I found in the primarily rural Neuse watershed (16,148 km^2) that discharge peaks on average increased under land use change by 5.3%, climate change by 54.7%, and the combined scenario by 61.7% under the 1% AEP precipitation event (Figure 10).

Notable exceptions to the finding that climate is the primary driver of increasing discharge trends exist. Specifically, Table C.5 suggests that land use change becomes the primary driver either where the watershed size is relatively small (<100 km^2) that makes urbanization become disproportionately impactful or the watershed is already densely urbanized, like in the Atlanta, Houston, and San Antonio metropolitan areas (Aboelnour et al., 2019; Lafontaine et al., 2015; Sebastian et al., 2019; Zhao et al., 2016). However, Table C.5 also finds that discharge trends in some urban metropolises, for example in watersheds near Las Vegas and Miami, are projected to be more influenced by climate change than land use change (Huq & Abdul-Aziz, 2021; Tong et al., 2016). The explanation for these exceptions could be attributed to the relative increases in urbanization and climate change expected in each watershed, and may require additional research to improve understanding of each drivers' variable influence.

The locations of change do not necessarily reflect floodplain extent, suggesting that hydrograph evaluation alone is not sufficient enough to provide insights into future hazards and hazard exposure. This finding also suggests that existing impervious surface has an important role in regulating the future influence of climate change and land use/land cover change on discharge trends. Climate change produced greater discharge responses than did land use/land cover at the HUC 6 to HUC 10 scale; however, this trend reversed locally within the City of Goldsboro by disproportionately increasing hazard extent and exposure. It is difficult to disentangle the principal component producing this effect since the City of Goldsboro is at a much smaller spatial scale than the City of Houston, the contributing area to

Goldsboro's tributaries (Little River, Big Ditch, and Stoney Creek) is smaller than major tributaries near Houston, and because this contributing area is more rural than the degree of the city's exurban sprawl. However, research conducted in the nearby Yadkin-Pee Dee Watershed of North Carolina reports discharge increasing at similar proportions to the findings of this research, which offers evidence that regional trends in climate and land use result in similar shifts to the hydrologic cycle (Suttles et al., 2018).

Duque et al. (2022) offer an interesting theory that could physically explain the non-linear increases in peak discharge under the combined climate change and LULCC scenario. First, the translation of rainfall into runoff shifts as climate change increases the frequency of flash flood-inducing precipitation and expands the wet season to later in the winter, which results in longer soil moisture retention: a phenomenon described as "system memory". Then, the translation of rainfall into runoff further shifts as LULCC limits infiltration and overland storage capacity via increased imperviousness and so too increases water routing efficiency via reduced surface roughness. The combination of these two shifts may be sufficient to shift the dynamic ratio of runoff to infiltration for all precipitation events, resulting in a non-linear amplification of peak discharge, timing, and volume. While the Vflo® model does not account for system memory during event-based simulations as in this research, this non-linear observation may be further exacerbated when running a continuous Vflo® model or another hydrologic model that specializes in soil moisture retention for balancing annual water budgets. I believe that the non-linear discharge increases that this research observes are the result of increasing extreme precipitation, which routinely exceeds the soil's infiltration capacity, and also decreasing surface roughness, which limits surface water storage. Other studies underscore the critical role that forested lands play in retaining stormwater, which is also likely important in the Neuse.

I also find that contributing area is an important predictor of discharge peak. As spatial changes occur heterogeneously across the watershed, variability in LULCC may be more important to understand how peak flows respond to concentrated development locally and may become more important for influencing peak discharge than climate change when less pervious landscapes are connected. I also

report predicted changes in floodplain extent in relation to the floodplain. Discharge peak increases projected under the RCP 8.5 and SSP 5 scenario result in an expansion of the 0.2% AEP floodplain in Little River by 0.5, 2, and 2.0%, in Big Ditch by 9.0%, 9.0%, and 16%, and in Stoney Creek by 72%, 59%, and 179% under the LULCC, CC, and combined scenarios, respectively (Figure 13). I find that these results further increase building exposure to the floodplain across Goldsboro by 3.0%, 10%, and 7.0% in Little River, 12%, 8.0%, and 13% in Big Ditch, and 332%, 271%, and 700% in Stoney Creek, respectively (Figure 13). These results are important for providing an upper estimate of floodplain area for the community, which signal that, depending on where people reside with respect to the floodplain, discharge trends are concerning for future flood exposure.

Model Limitations

There are several limitations to the model results. First, any model uncertainty in the ICLUS and CMIP5 datasets are propagative in the model framework. The ICLUS model projects land use changes as the result of predicted population growth, assumptions of land use zoning, and socio-economic drivers that may be inaccurate in the long term even if they are reasonably accurate in the near term (Prestele et al., 2016). The CMIP5 model ensemble predicts global climate variables daily through the end of the century, and the assumptions that predicate each model, inter-model variability, and overall accuracy are explored elsewhere (Knutti & Sedláček, 2013; Liu et al., 2014; C. Wang et al., 2014). However, it is important to note that deriving specific weather events from multi-decadal climatic trends is not representative of future variability. Here, my decision to consider the median of all 20 CMIP5 model outputs assumes that I weigh the predictive ability of each model equally, when I am uncertain whether any of the models will perform well over time. Future work can quantify these uncertainties by assessing which models have most consistently predicted extreme precipitation since 2005 and proportionally weigh their relative influence.

Second, I chose to use a 50-year moving window approach and a Gumbel GEVD to predict the future AEP precipitation event volume. While the 30-year approach is common and is shown in Appendix

A, I opted for a longer moving window to reduce short-term variability in climate projections. I also recognize that future precipitation may not fit the Gumbel distribution as future precipitation extremes may become more tail dependent, which is not well represented by the Gumbel. Other research has considered the L-moment or the Weibull distribution for future extreme precipitation (Pokhrel et al., 2020). My research also assumes an SCS Type II distribution for precipitation, which defines the sub-daily distribution of rainfall for the inland United States (USDA, 1986). While this distribution is appropriate for small watersheds in the study region, it is unknown whether and how the sub-daily distribution of rainfall will change (Awadallah et al., 2016). Future work could determine model sensitivity to different rainfall intensities or consider the impact of different IDF curves.

Third, there are also uncertainties that arise from the model framework. Decisions concerning reservoir releases are difficult to model in Vflo®, the use of rating curves for calibration and validation is limited to gaged locations, and the physical representation of hysteresis is not preserved in Vflo®, thus making it difficult to match the receding limb of the observed storm hydrograph. A single pair of rating curves defines the stage-storage and stage-discharge relationship at Falls Dam, which prevents the model from capturing variations determined by operating procedures that control dam releases by limiting flooding downstream. Vflo® routes water using the Kinematic Wave approximation of the shallow water equations by conserving mass but not momentum. As such, backwater effects are not captured and result in uncharacteristically efficient channel hydrologic routing. This limitation is difficult to resolve without using a different hydrologic model or measuring stage discharge and stage storage relationships in ungaged locations, which was outside of the project scope. This is particularly important for considering the appropriateness of reporting changes in peak discharge at locations that were not explicitly calibrated (ie. at USGS stations), and likely explains negative non-linear outliers in Figure 8. I chose to proceed with the Vflo® model because the model excels at defining distributed land cover and soil infiltration, despite these concerns.

Policy Recommendations

Floods pose risks to individuals, communities, and critical infrastructure. This is particularly concerning for communities along large rivers, especially in coastal plain regions that are susceptible to heavy mesoscale convective systems and tropical cyclones events. The risk of these flood hazards is further amplified because of the population density and low-lying landscape of coastal regions. Cities along large rivers like Goldsboro must also contend with positive trends in discharge that yield increasing fluvial hazards (Archfield et al., 2016; Dethier et al., 2020). Consequently, these discharge trends are predicted to further intensify as climate change impacts storm magnitude and frequency.

Policy recommendations consistent with these findings include the reassessment of land use zoning policy along the floodway and floodplain fringe, the incorporation of model frameworks like the one demonstrated in this research into Strategic Plans at the city or watershed scale, and the distribution and dissemination of projected flood hazard maps as a science communication and risk assessment tool. My research finds that LULCC has a disproportionate impact on regulating discharge where impervious surface increases are relatively large and physically connected, making land use zoning policy crucial for limiting the increase in hazard magnitude and frequency at a local level. Brody et al. (2017) found that large, contiguous, natural open spaces yield flood mitigation benefits, which leads me to recommend maintaining such lands across the watershed, especially forested and wetland areas in rural settings and passive agricultural lands in more urban environments as suggested by Brody et al. (2014). Floodplain maps frequently underestimate current flood hazards due to incomplete data and intermittent updates (Pricope et al., 2022). Municipalities concerned with future flooding can choose to enact modeling frameworks like this one to determine more stringent development regulations that target the reduction of flood exposure. Individuals informed of their property's flood risk are additionally more likely to proactively engage in risk management, knowledge that is often communicated through engagement (Mojtahedi & Oo, 2017).

Conclusion

This study evaluates the independent and combined effects of climatic and land cover changes on trends in watershed hydrology and flood hazards to understand the role that each driver poses in the near future. I model changes in stormwater peak flows, flood depth and extent and quantify the 20%, 10%, 2.0%, 1.0%, and 0.2% annual exceedance probability 24-hour design storms for discharge over the 21st century. Near Goldsboro, future LULCC and CC result in an increase in peak discharge by 51.1%, 74.4%, 87.6%, 79.3%, and 68.4% with respect to the 20%, 10%, 2.0%, 1.0%, and 0.2% annual exceedance probability 24-hour design storms. I find that the effects of climate change on peak streamflow are greater than the effects of land use/land cover change. The effect of combining both climate change and LULCC drivers on peak discharge is often greater than the sum of their independent effects and at sub-watershed outlets can result in up to a 7% peak discharge excess over the sum of each driver's peak discharge.

Peak flows are input to three Hydrologic Engineering Center River Analysis System models for the City of Goldsboro to assess changes in flood extent and building exposure over the 21st century. The influence of hydrologic peak changes on floodplain extent varies considerably across the City of Goldsboro. In the Big Ditch tributary, future LULCC and CC result in an increase in hazard area by 13.3%, 11.4%, 15.5%, 14.4%, and 15.5% with respect to the 20%, 10%, 2.0%, 1.0%, and 0.2% annual exceedance probability 24-hour design storms. These projections would result in an increase in building exposure by 13.6%, 10.3%, 13.4%, 13.1%, and 12.7%, respectively. In the Little River tributary, the 20%, 10%, 2.0%, 1.0%, and 0.2% annual exceedance probability 24-hour design storms lead to hazard area increases of 6.0%, 4.1%, 2.0%, 1.7%, and 1.5% and result in building exposure increases of 22.8%, 9.6%, 8.3%, 8.5%, and 7.1%. Finally, hazard area increases in the Stoney Creek tributary of 117%, 115%, 123%, 134%, and 179% respectively result in building exposure increases of 729%, 757%, 607%, 598%, and 700%.

My findings have important implications for informing city and regional planning efforts to constrain the potential hydrologic impacts of land use decisions as well as provide residents with spatiotemporal

hazard projections so that they may understand their property's evolving flood risk. These changes in flood hazard have implications in the near term because they can inform individuals who reside outside of the effective floodplain, who do not have flood insurance, but are predicted to be exposed to this natural hazard.

APPENDIX A. CLIMATE MODEL WINDOWS

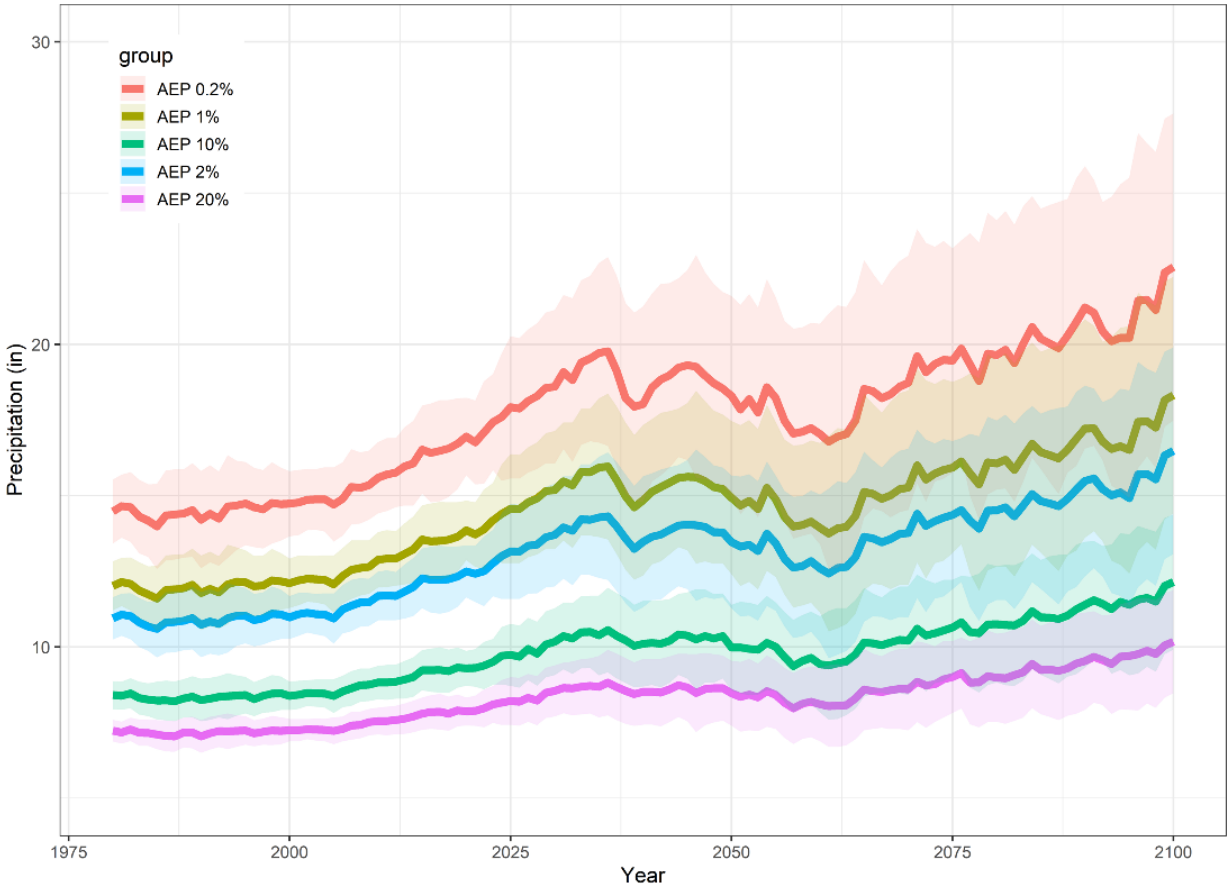

Figure 14. Annual maximum precipitation using a 30-year moving window.

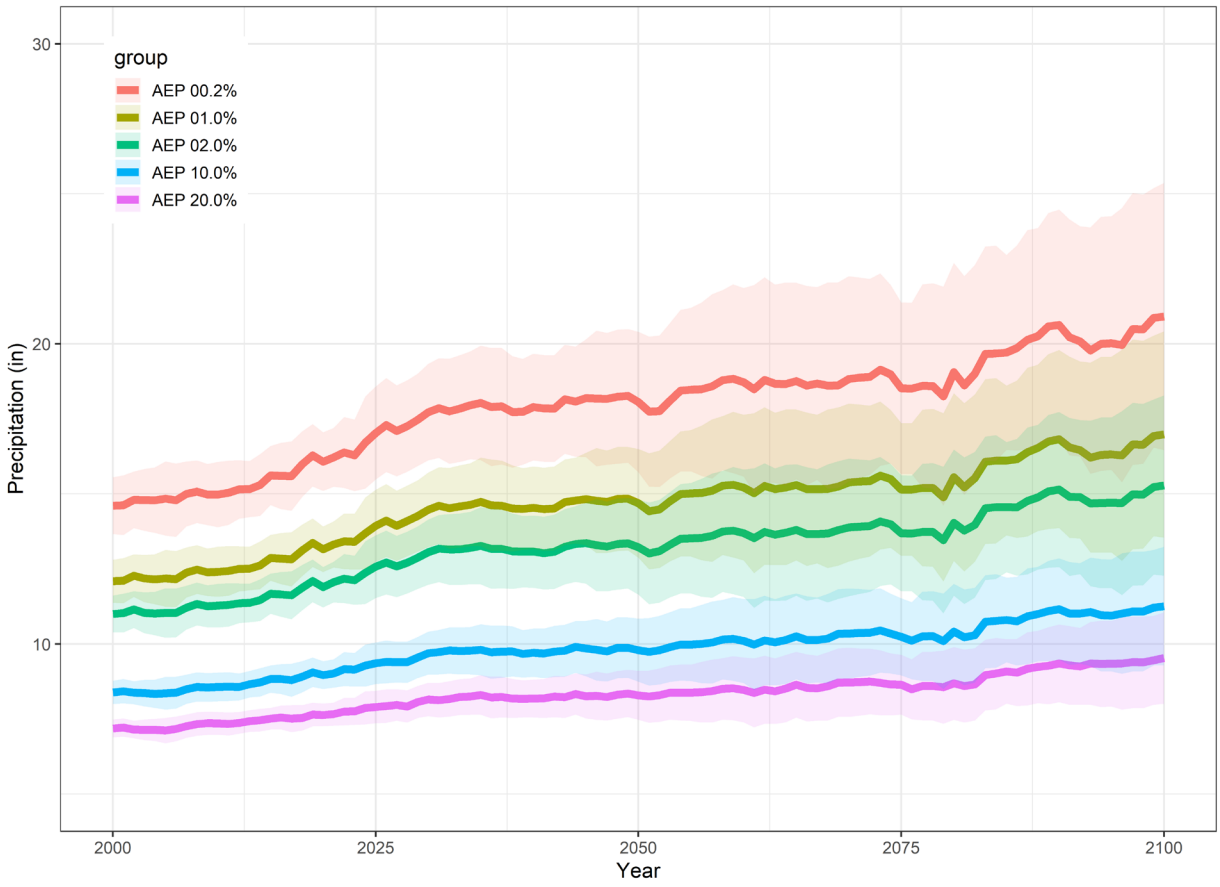

Figure 15. Annual maximum precipitation using a 50-year moving window.

APPENDIX B. ADDITIONAL TABLES

Table 3. Model Comparison for LULCC Projections modified from Sohl et al. (2016).

Model Name	Temporal Coverage	Time Step	Spatial Resolution	Thematic Resolution	Geographic Coverage	Scenarios
FORE-SCE[a]	1992-2100	Annual	250 m	17 classes	CONUS	4
NRI[b]	2001-2051	Start, End	100 m	5 classes	CONUS	5
FS-RPA[c]	1997-2060	Decadal	County	5 classes	CONUS	3
ICLUS[d]	1970-2100	Decadal	100 m	18 classes	CONUS	4
IMAGE SRES[e]	1970-2100	Decadal	0.5º	19 classes	Global	4
IMAGE OECD[f]	1970-2100	5 Years	0.5º	19 classes	Global	5
RCP[g]	2005-2100	Decadal	0.5º	Variable	Global	4
GCAM CONUS[h]	2005-2095	Annual	0.05º	19 classes	CONUS	3

[a] Sohl et al. (2016); [b] Lawler et al. (2014); [c] Wear (2013); [d] Bierwagen et al. (2010); [e] Strengers et al. (2004); [f] Alkemade et al. (2012); [g] Hurtt et al. (2011); [h] West and Le Page (2014)

Table 4. Reclassification of ICLUS land uses into land cover percent imperviousness.

Code	Imperviousness	ICLUS Description	Reference Description
0	0.00	natural water	NA
1	0.00	reservoir/canal	NA
2	0.01[a]	wetland emergent	herbaceous wetland[a]
3	0.09 [a]	recreation/conservation	other grasses
4	0.05 [a]	timber	mixed forest
5	0.05 [a]	grazing	hay/pasture
6	0.05 [a]	pasture	hay/pasture
7	0.08 [a]	cropland	row crops
8	0.17 [a]	mining/barren land	transitional barren
9	0.09 [a]	parks/golf course	other grasses
10	0.12 [b]	exurban/low density	residential; 1/2-ac lot
11	0.21 [b]	exurban/high density	residential; 1/4-ac lot
12	0.28 [b]	suburban	residential; 1/8-ac lot
13	0.42 [a]	urban/low density	low density residential
14	0.77 [a]	urban/high density	high density residential
15	0.57 [a]	commercial	commercial/industrial
16	0.57 [a]	industrial	commercial/industrial
17	0.35 [b]	institutional	industrial; office
18	0.81 [b]	transportation	streets and easements

[a] values obtained from Exum et al. (2005)

[b] values obtained from Zuellig et al. (2008)

Table 5. Reclassification of ICLUS land uses into land cover Manning's roughness.Source: Kalyanapu et al.(2009)).

Code	Roughness	ICLUS Description	Reference Description
0	0.0010	natural water	open water
1	0.0010	reservoir/canal	open water
2	0.1825	wetland	emergent herbaceous wetlands
3	0.0404	recreation/conservation	developed/open space
4	0.4000	timber	mixed forest
5	0.3680	grazing	grassland/herbaceous
6	0.3250	pasture	pasture/hay
7	0.3250	cropland	cultivated crops
8	0.0113	mining/barren land	barren land
9	0.0404	parks/golf course	developed/open space
10	0.0678	exurban/low density	developed/low intensity
11	0.0678	exurban/high density	developed/medium intensity
12	0.0678	suburban	developed/medium intensity
13	0.0404	urban/low density	developed/medium intensity
14	0.0404	urban/high density	developed/high intensity
15	0.0404	commercial	developed/high intensity
16	0.0404	industrial	developed/high intensity
17	0.0404	institutional	developed/high intensity
18	0.0404	transportation	developed/high intensity

Table 6. ICLUS-predicted land use change from 2020 to 2100. Net loss of land area is represented in red on the far-right column.

Land Use	Land Use Gains (km2)	Land Use Losses (km2)	Net Change (km2)
Commercial	127	-	127
Exurban High Density	1280	852	428
Exurban Low Density	635	898	-263
Industrial	39.4	-	39.3
Suburban	1109	441	668
Urban High Density	65.1	0.78	64.3
Urban Low Density	835	104	731
Cropland	-	845	-845
Grazing	-	32	-32
Pasture	-	3.59	-3.59
Timber	-	810	-810
Wetlands	-	104	-104

Table 7. CMIP5-predicted rainfall volumes from 2000 to 2100. Projections are determined using an ensemble of 20 CMIP5 models with a gumbel distribution and a 50-year moving window.

Year	20% AEP (cm)	10% AEP (cm)	2% AEP (cm)	1% AEP (cm)	0.2% AEP (cm)
2000	18.2	21.3	27.9	30.7	37.1
2010	18.6	21.7	28.6	31.5	38.0
2020	19.4	22.7	30.2	33.4	40.8
2030	20.7	24.6	33.1	36.7	45.0
2040	20.7	24.6	33.2	36.9	45.4
2050	21.0	24.8	33.5	37.3	45.8
2060	21.5	25.6	34.7	38.6	47.5
2070	22.1	26.2	35.2	39.0	47.8
2080	22.0	26.4	35.6	39.5	48.4
2090	23.7	28.3	38.4	42.7	52.3
2100	24.2	28.6	38.8	43.1	53.1

Table 8. Literature review of trends in scenario-based discharge projections. The Neuse River watershed is predicted to respond to LULCC, CC, and their combined effects similarly to the Las Vegas Wash of Nevada and the Yadkin-Pee Dee of North Carolina.

Watershed	**Drainage Area (km^2)**	**Temporal Range**	**Discharge % Increase**		
			LULCC	CC	Combo
[1] **Little Eagle, IN**	75	1992 to 2011	27	23	46
[2] **Hinkson, MO**	231	2018 to 2050	2	12	14
[3] **Conestoga, PA**	1,217	1970-1999 to 2025-2034	0.4	10	-
[4] **Buffalo-San Jacinto, TX**	2,531	1900 to 2017	54	20	84
[5] **Las Vegas Wash, NV**	4,855	2010 to 2050	5	43	59
[6] **Southeast Coasts, FL**	7,117	2010 to 2080	26	87	118
[7] **San Antonio, TX**	10,826	2020-2049 to 2070-2099	47	-	58
Neuse, NC	16,149	2020 to 2100	5	55	62
[8] **Yadkin-Pee Dee, NC**	17,780	1992 to 2060	6-24	13-43	4-63
[9] **Puget Sound, WA**	31,000	1970-2000 to 2050	6	9	-
[10] **Apalachicola-Chattahoochee-Flint, GA**	50,700	2000 to 2090	-	20	83

[1] Aboelnour et al., (2019); [2] Sunde et al., (2018); [3] Chang et al., (2003); [4] Sebastian et al., (2019); [5] Tong et al., (2016); [6] Huq & Abdul-Aziz, (2021); [7] Zhao et al., (2016); [8] Suttles et al., (2018); [9] Cuo et al., (2011); [10] Lafontaine et al., (2015)

APPENDIX C. ADDITIONAL FIGURES

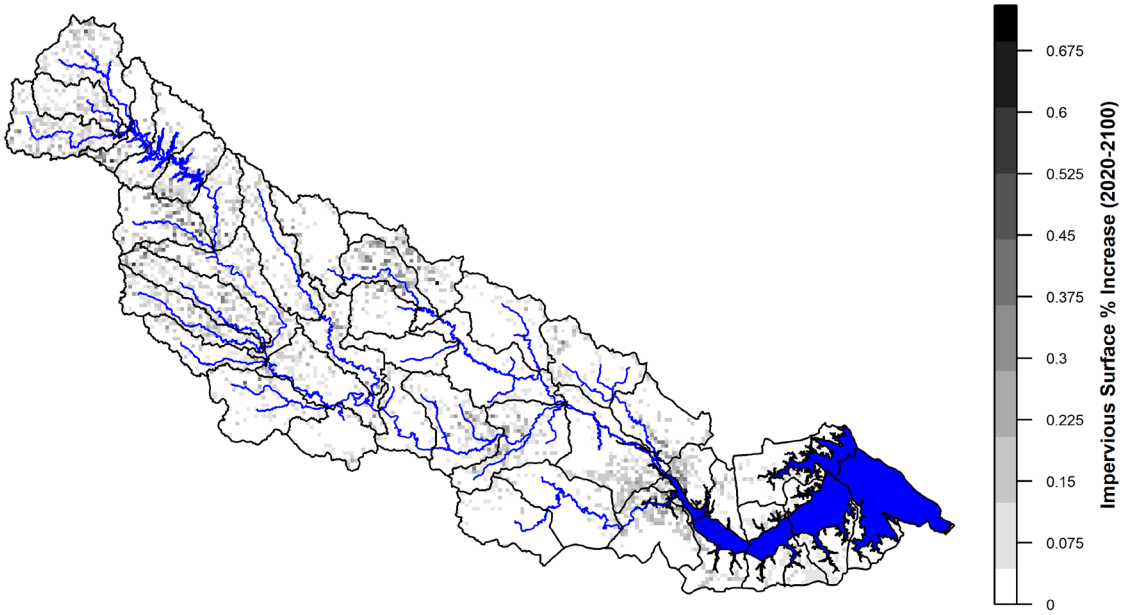

Figure 16. Impervious surface increases between 2020 and 2100 in the Neuse River watershed. The ICLUS model predicts the greatest relative increase in impervious surfaces to be along urban corridors, primarily between Raleigh and Smithfield in the NW, Wilson in the N, Kinston in the S, and New Bern in the SE of the watershed. Urban growth is predicted to primarily be urban sprawl as opposed to urban infilling, consistent with the SSP5 scenario.

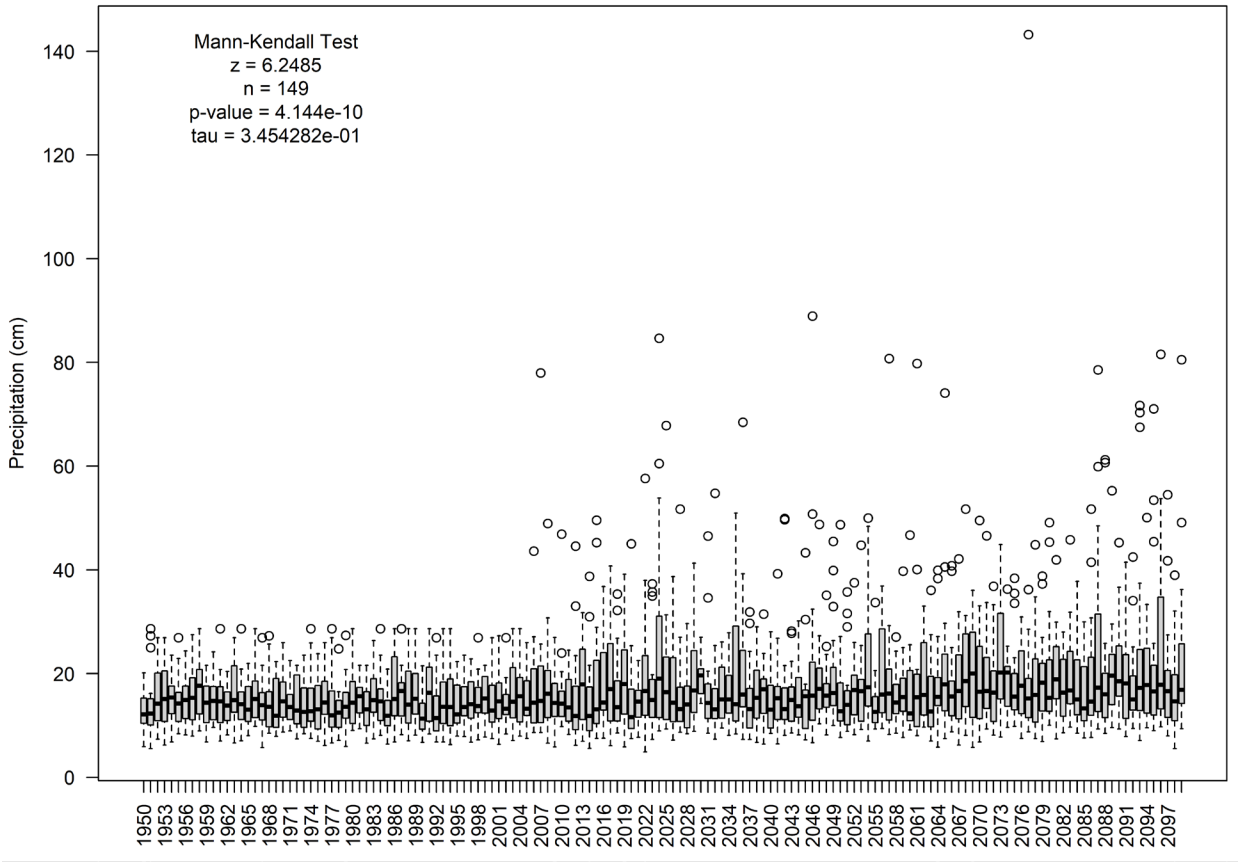

Figure 17. CMIP5-predicted annual daily maximum precipitation. Thick horizontal lines represent the median, the grey box represents the first and third quartiles, and the whiskers represent the minimum and maximum of the data set. Empty circles represent outliers. Under a Mann-Kendall test, we find that there is a significant monotonic trend in the median annual daily maximum precipitation is at a 95% confidence interval because our p-value of 4.1e-10 is less than 0.05. We also find that this trend is increasing since our tau is positive (3.45e-01). The CMIP5 model ensemble agree that an overall increase in precipitation volume will occur by the end of the century, with an average annual increase of 0.35 cm per year.

APPENDIX D. RATING CURVES

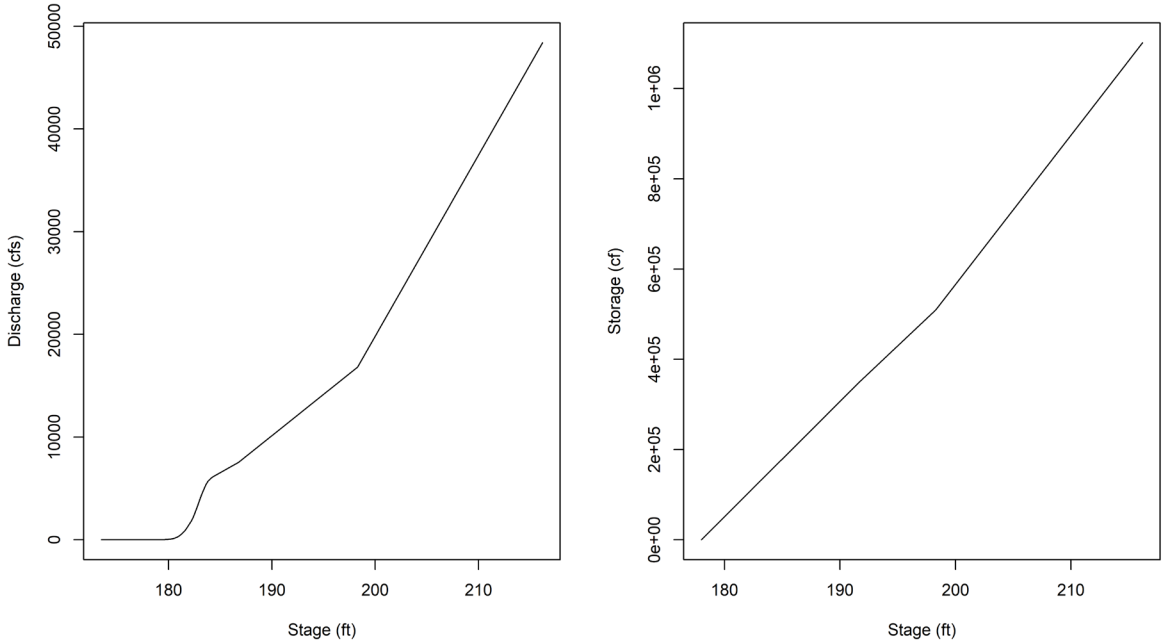

Figure 18. Rating Curves at USGS 02087183.

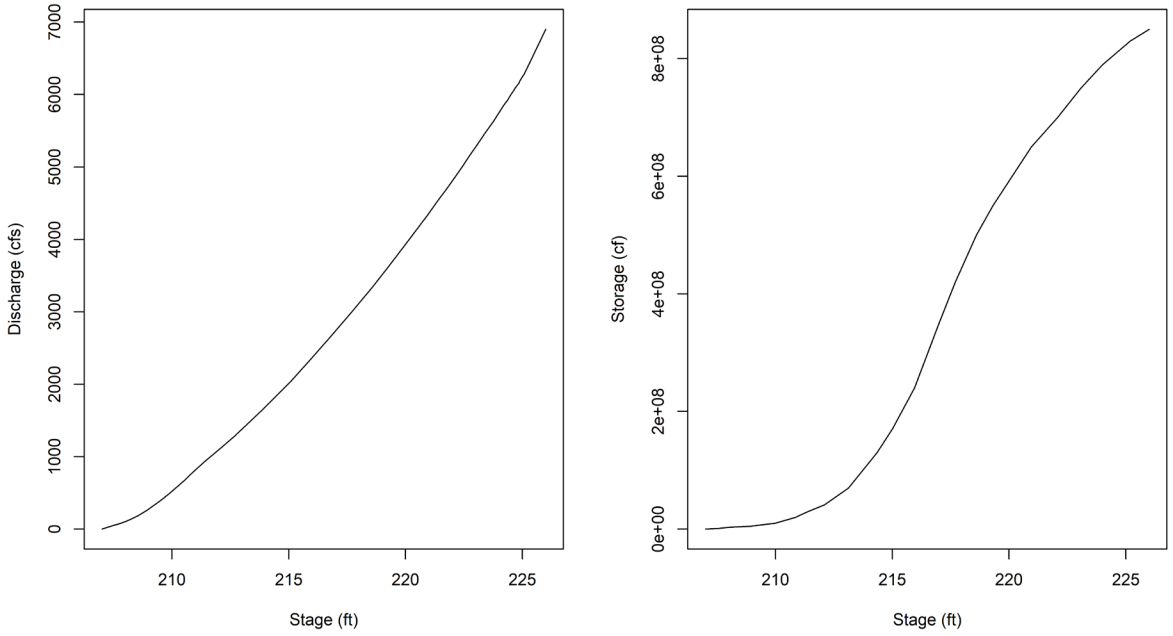

Figure 19. Rating Curves at USGS 02087275.

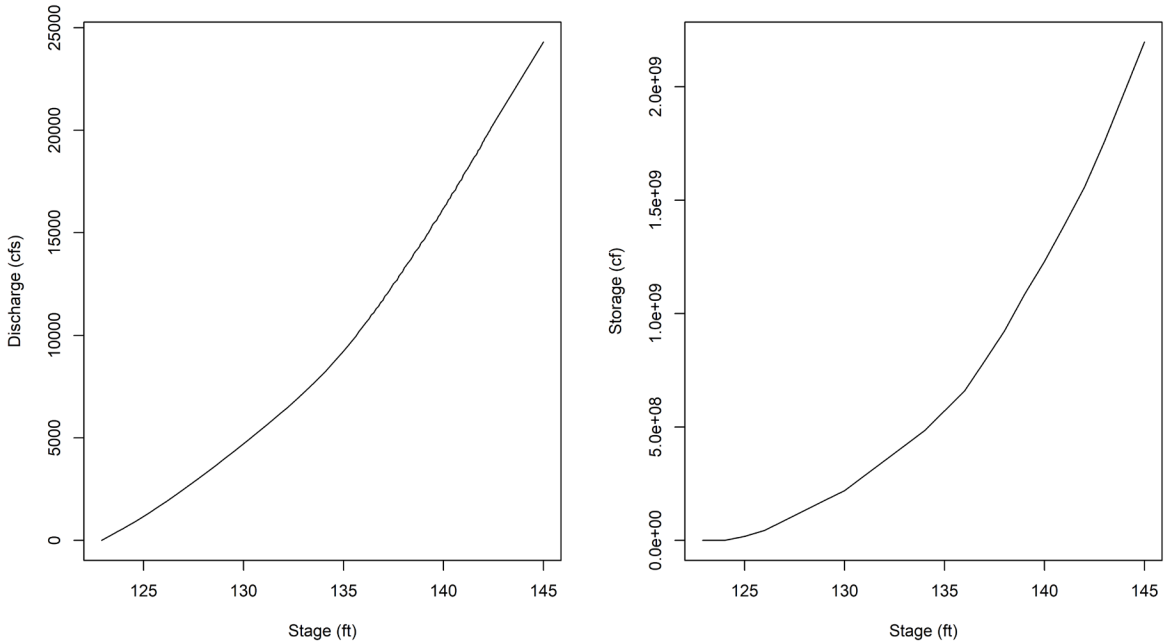

Figure 20. Rating Curves at USGS 02087275.

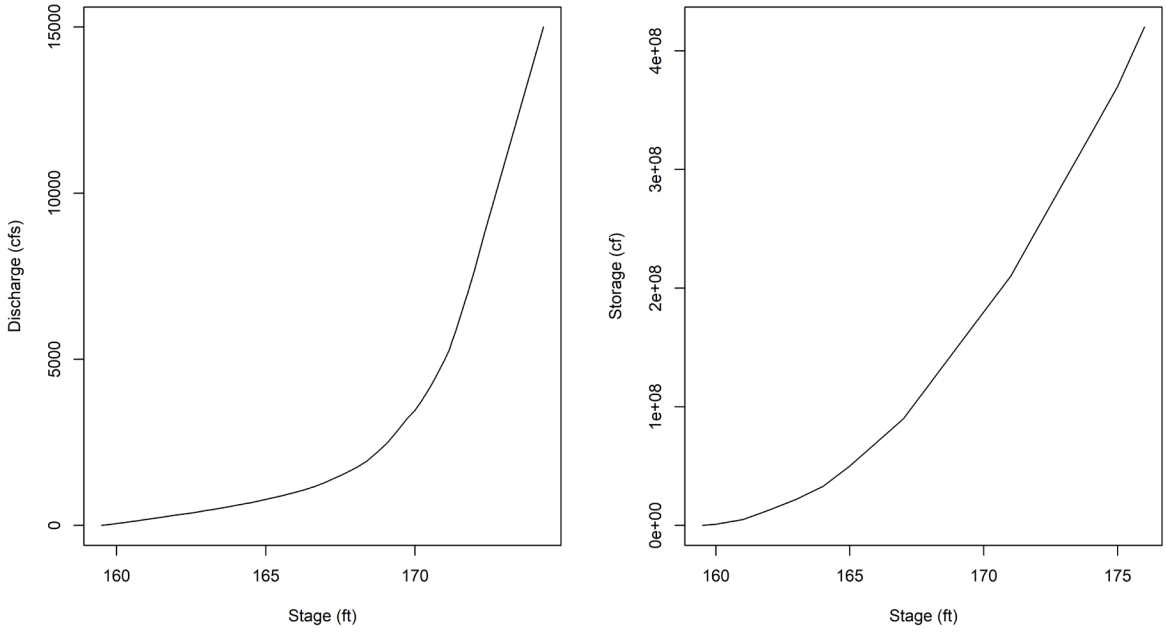

Figure 21. Rating Curves at USGS 02088000.

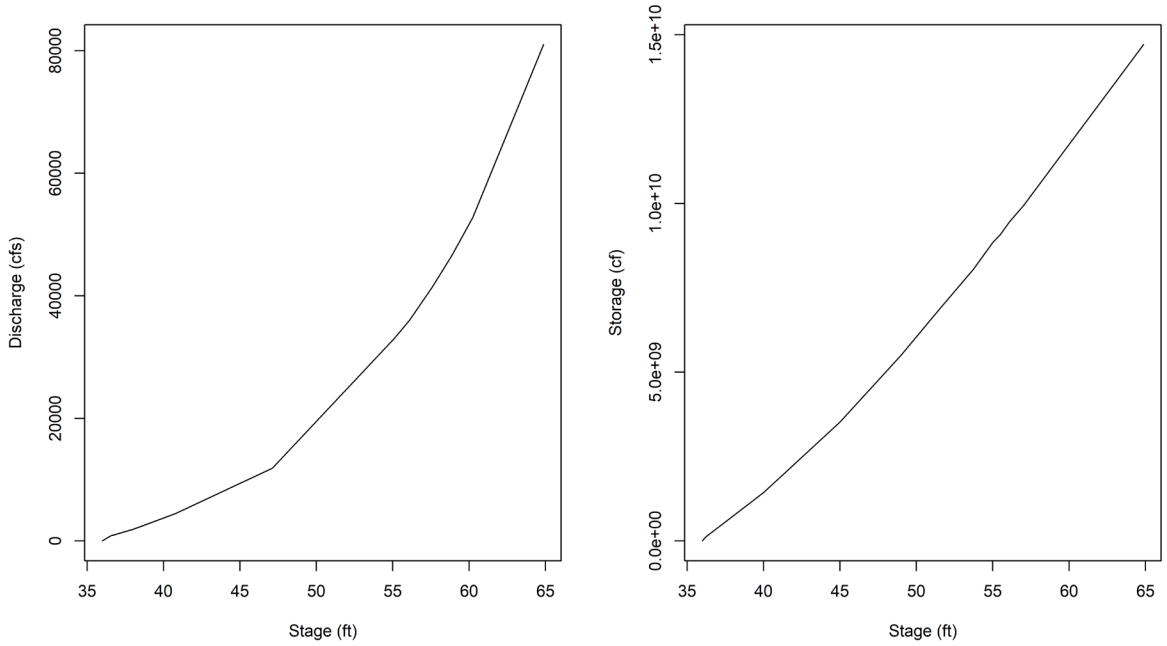

Figure 22. Rating Curves at USGS 02089000.

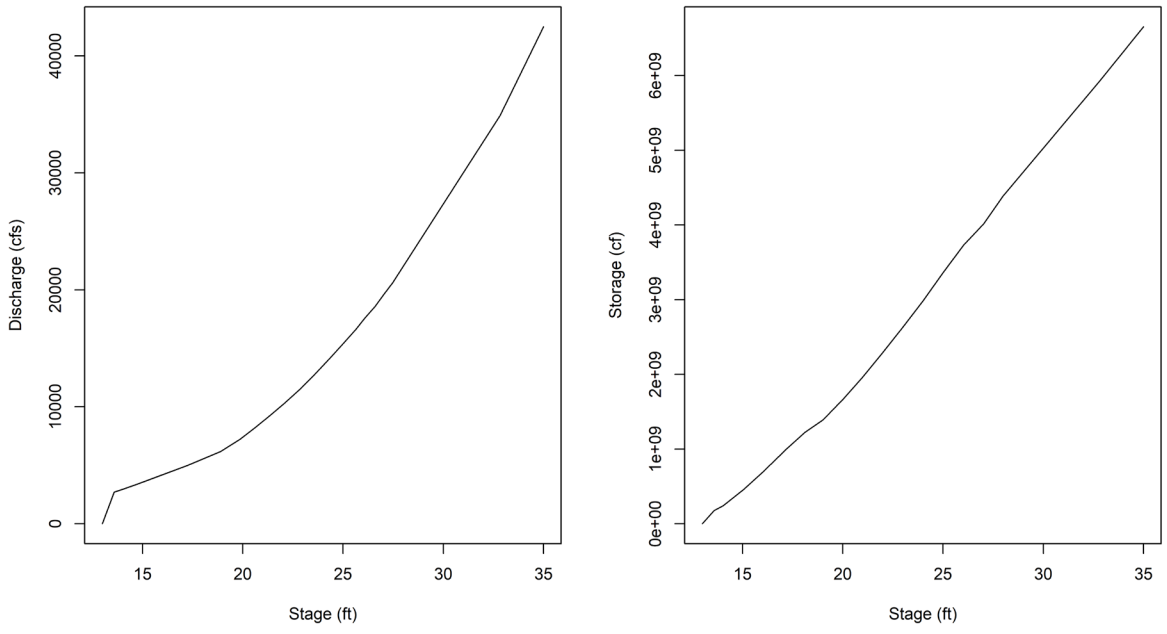

Figure 23. Rating Curves at USGS 02089500.

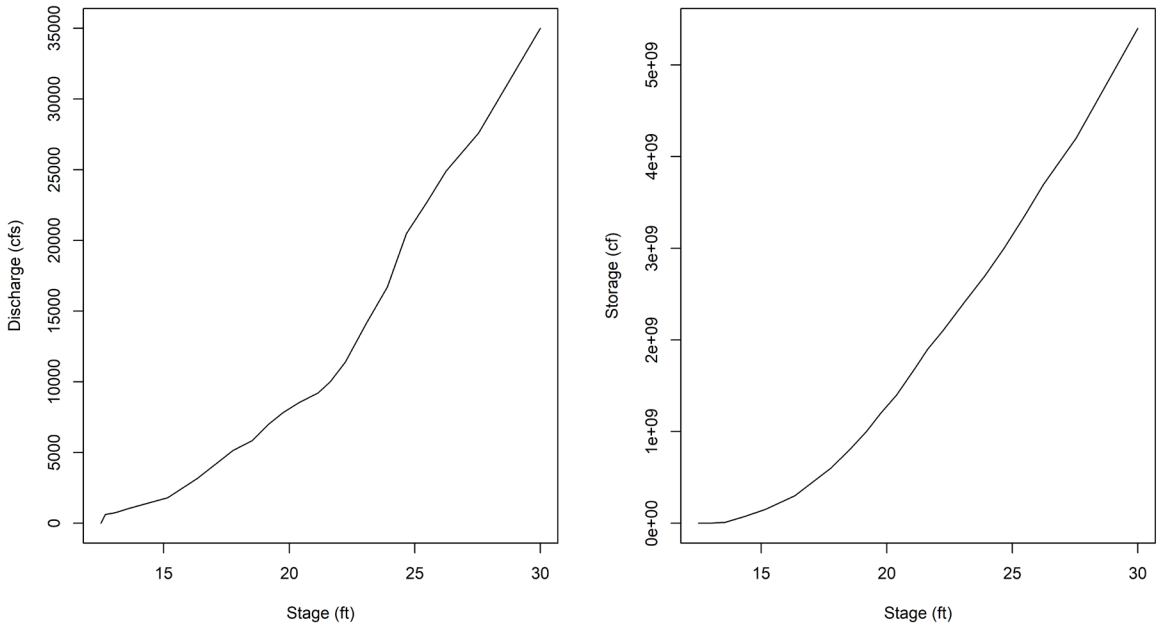

Figure 24. Rating Curves at USGS 02091500.

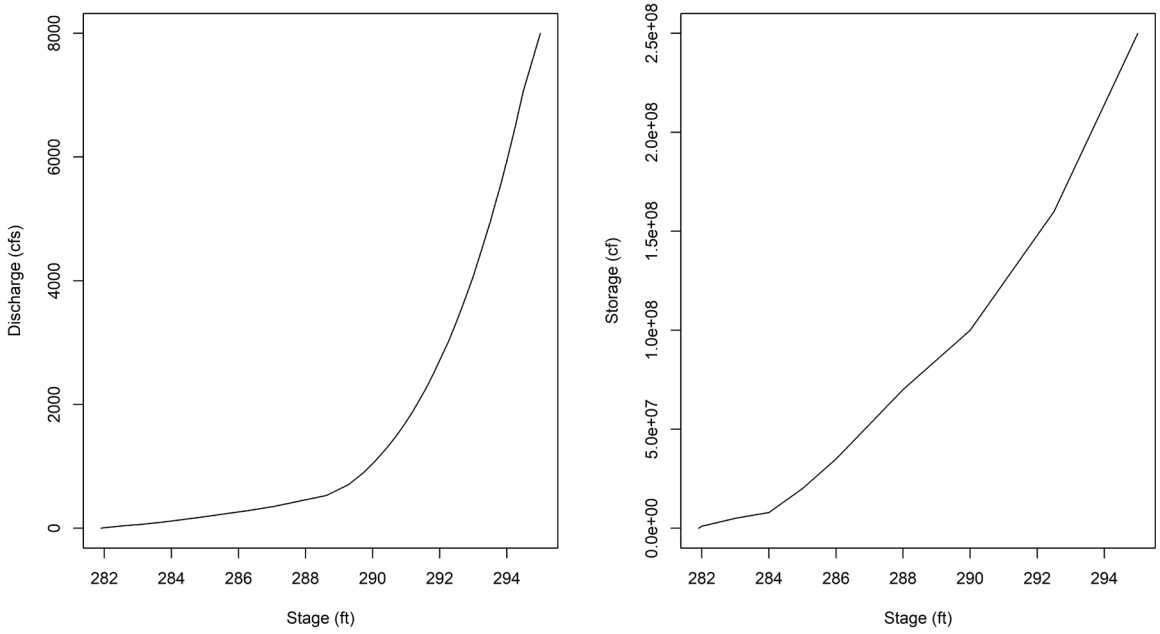

Figure 25. Rating Curves at USGS 0208758850.

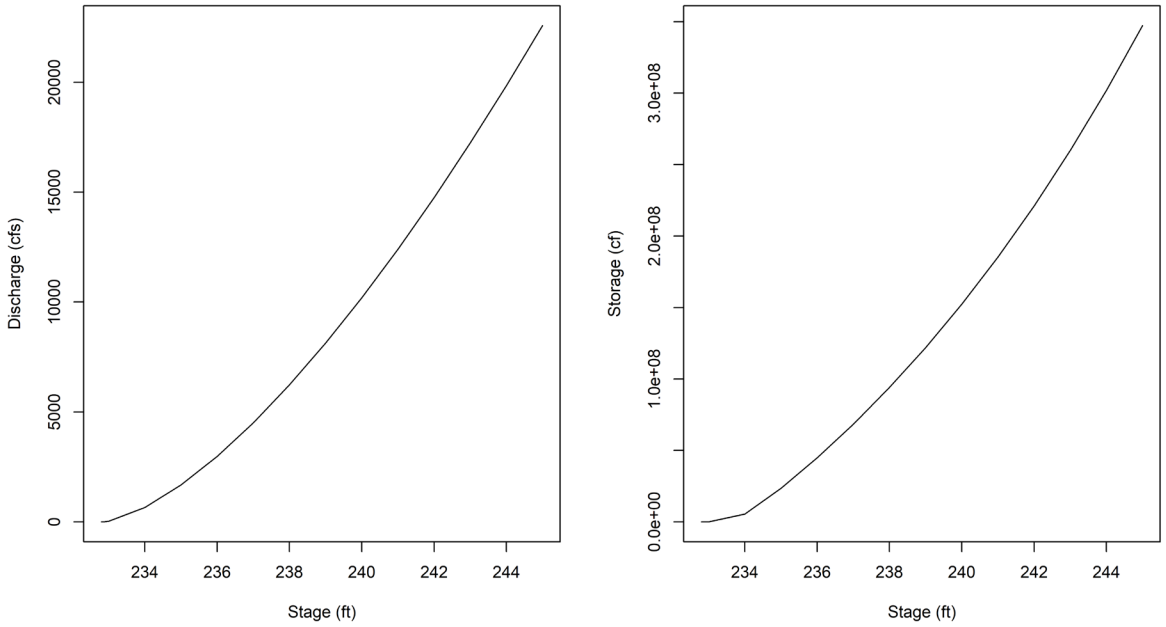

Figure 26. Rating Curves at Lake Benson.

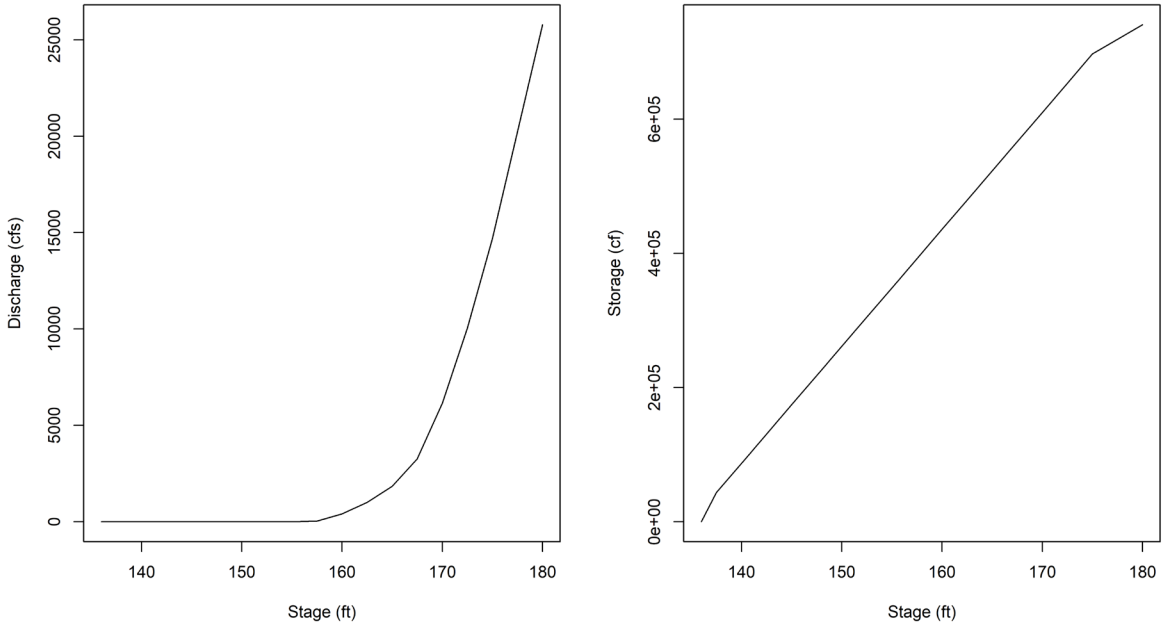

Figure 27. Rating Curves at Town of Beulah.

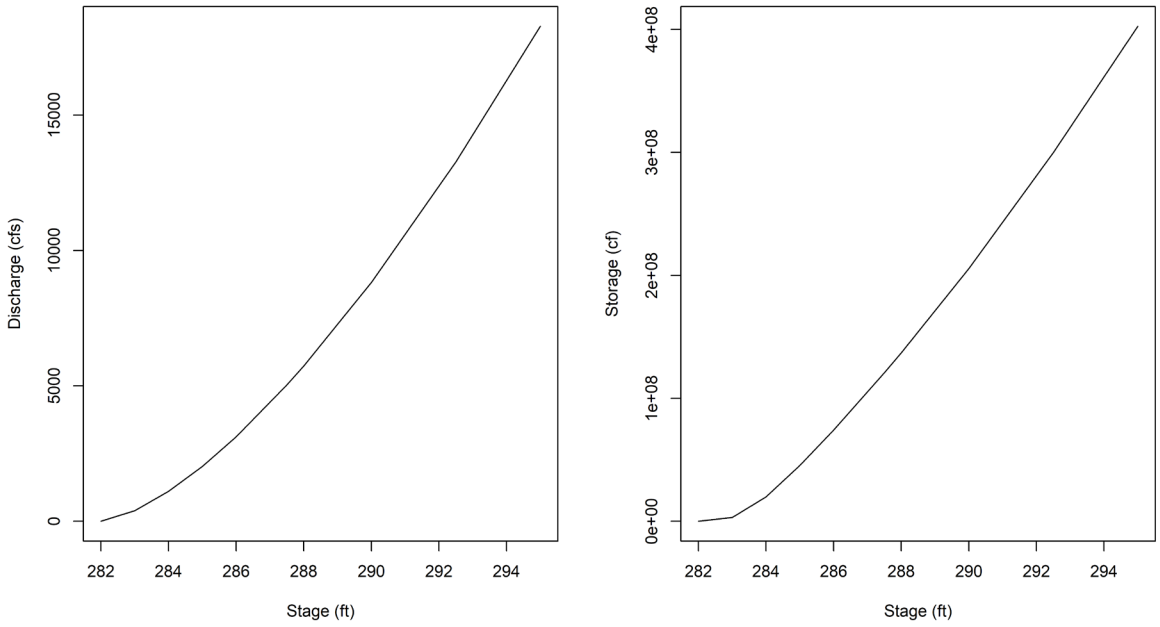

Figure 28. Rating Curves at Lake Wheeler.

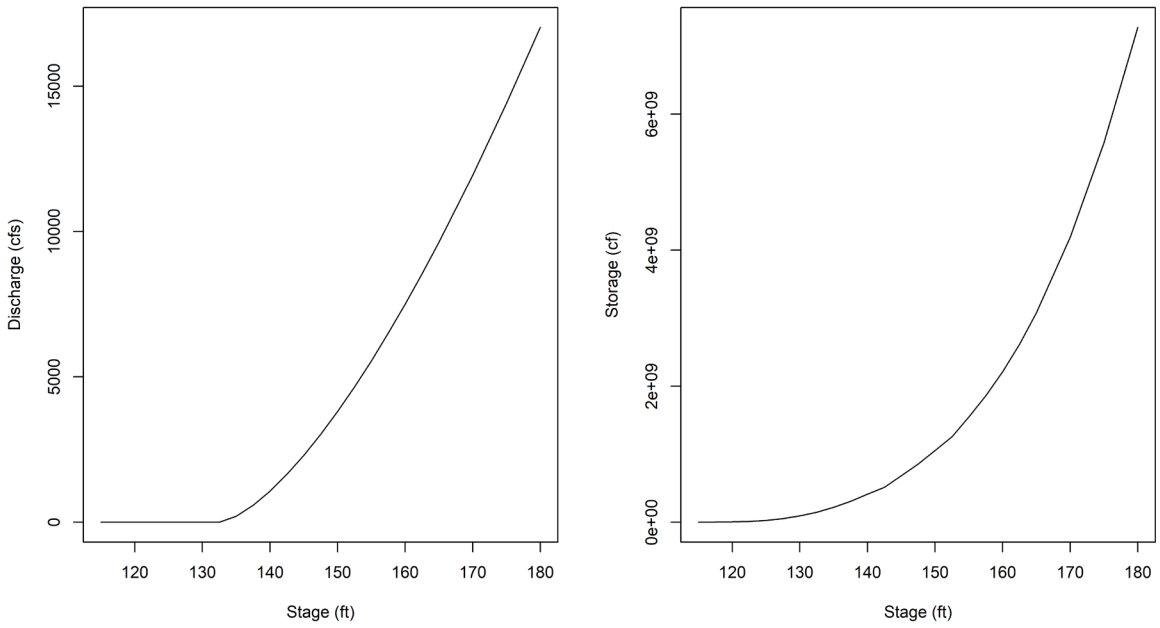

Figure 29. Rating Curves at Town of Wilson Mills.

REFERENCES

Abatzoglou, J. T., & Brown, T. J. (2012). A comparison of statistical downscaling methods suited for wildfire applications. *International Journal of Climatology*, *32*(5), 772–780. https://doi.org/10.1002/joc.2312

Aboelnour, M., Gitau, M. W., & Engel, B. A. (2019). Hydrologic response in an urban watershed as affected by climate and land-use change. *Water (Switzerland)*, *11*(8). https://doi.org/10.3390/w11081603

Akter, T., Quevauviller, P., Eisenreich, S. J., & Vaes, G. (2018). Impacts of climate and land use changes on flood risk management for the Schijn River, Belgium. *Environmental Science and Policy*, *89*(August), 163–175. https://doi.org/10.1016/j.envsci.2018.07.002

Aliyari, F., Bailey, R. T., & Arabi, M. (2021). Appraising climate change impacts on future water resources and agricultural productivity in agro-urban river basins. *Science of the Total Environment*, *788*. https://doi.org/10.1016/j.scitotenv.2021.147717

Alkemade, R., Bouwman, L., Biemans, H., de Elzen, M., Hilderink, H., Klein Goldewijk, K., Kram, T., Lucas, P., Olivier, J., Stehfest, E., & van Vuuren, D. (2012). *The IMAGE model suite used for the OECD Environmental Outlook to 2050*.

Allan, R. P., & Soden, B. J. (2008). Atmospheric warming and the amplification of precipitation extremes. *Science*, *321*(5895), 1481–1484. https://doi.org/10.1126/science.1160787

Archfield, S. A., Hirsch, R. M., Viglione, A., & Blöschl, G. (2016). Fragmented patterns of flood change across the United States. *Geophysical Research Letters*, *43*(19), 10,232-10,239. https://doi.org/10.1002/2016GL070590

Arnell, N. W., & Gosling, S. N. (2016). The impacts of climate change on river flood risk at the global scale. *Climatic Change*, *134*(3), 387–401. https://doi.org/10.1007/s10584-014-1084-5

Awadallah, A. G., Saad, H., Elmoustafa, A., & Hassan, A. (2016). Reliability assessment of water structures subject to data scarcity using the SCS-CN model. *Hydrological Sciences Journal*, *61*(4), 696–710. https://doi.org/10.1080/02626667.2015.1027709

Barsugli, J. J., Guentchev, G., Horton, R. M., Wood, A., Mearns, L. O., Liang, X.-Z., Winkler, J. A., Dixon, K., Hayhoe, K., Rood, R. B., Goddard, L., Ray, A., Buja, L., & Ammann, C. (2013). The Practitioner's Dilemma: How to Assess the Credibility of Downscaled Climate Projections. *EOS*, *94*(46), 424–425.

Bedient, P., Huber, W., & Vieux, B. (2008). *Hydrology and Floodplain Analysis* (H. Stark, Ed.; 6th ed.). Pearson.

Berndtsson, R., Becker, P., Persson, A., Aspegren, H., Haghighatafshar, S., Jönsson, K., Larsson, R., Mobini, S., Mottaghi, M., Nilsson, J., Nordström, J., Pilesjö, P., Scholz, M., Sternudd, C., Sörensen, J., & Tussupova, K. (2019). Drivers of changing urban flood risk: A framework for action. *Journal of Environmental Management*, *240*(October 2018), 47–56. https://doi.org/10.1016/j.jenvman.2019.03.094

Beven, J. L., Berg, R., & Hagen, A. (2019). *National Hurricane Center Tropical Cyclone Report: Hurricane Michael (AL142018)*.

Bierwagen, B. G., Theobald, D. M., Pyke, C. R., Choate, A., Groth, P., Thomas, J. v., & Morefield, P. (2010). National housing and impervious surface scenarios for integrated climate impact

assessments. *Proceedings of the National Academy of Sciences of the United States of America*, *107*(49), 20887–20892. https://doi.org/10.1073/pnas.1002096107

Birkland, T. A., Burby, R. J., Conrad, D., Cortner, H., & Michener, W. K. (2003). River Ecology and Flood Hazard Mitigation. *Natural Hazards Review*, *4*(1), 46–54. https://doi.org/10.1061/(asce)1527-6988(2003)4:1(46)

Blöschl, G. (2022). Three hypotheses on changing river flood hazards. *Hydrology and Earth System Science*. https://doi.org/10.5194/hess-2022-232

Boggs, J. L., & Sun, G. (2011). Urbanization alters watershed hydrology in the Piedmont of North Carolina. *Ecohydrology*, *4*(2), 256–264. https://doi.org/10.1002/eco.198

Bradshaw, C. J. A., Sodhi, N. S., Peh, K. S. H., & Brook, B. W. (2007). Global evidence that deforestation amplifies flood risk and severity in the developing world. *Global Change Biology*, *13*(11), 2379–2395. https://doi.org/10.1111/j.1365-2486.2007.01446.x

Brody, S., Blessing, R., Sebastian, A., & Bedient, P. (2014). Examining the impact of land use/land cover characteristics on flood losses. *Journal of Environmental Planning and Management*, *57*(8), 1252–1265. https://doi.org/10.1080/09640568.2013.802228

Brody, S. D., Highfield, W. E., Blessing, R., Makino, T., & Shepard, C. C. (2017). *Evaluating the effects of open space configurations in reducing flood damage along the Gulf of Mexico coast*. https://doi.org/10.1016/j.landurbplan.2017.07.003

Bruno, M., Bloschl, G., Vorogushyn, S., Dottori, F., Aerts, J., Bates, P., Bertola, M., Kemter, M., Kreibich, H., Lall, U., & Macdonald, E. (2021). Causes, impacts and patterns of disastrous river floods. *Nature Reviews*.

Butler, D., & Davies, J. W. (2011). *Urban Drainage* (3rd ed.). Spon Text.

Caldwell, P. v., Sun, G., McNulty, S. G., Cohen, E. C., & Moore Myers, J. A. (2012). Impacts of impervious cover, water withdrawals, and climate change on river flows in the conterminous US. *Hydrology and Earth System Sciences*, *16*(8), 2839–2857. https://doi.org/10.5194/hess-16-2839-2012

Carter, L. M., Terando, A., Dow, K., Hiers, K., Kunkel, K. E., Lascurain, A., Marcy, D. C., Osland, M. J., & Schramm, P. J. (2018). *Chapter 19 : Southeast. Impacts, Risks, and Adaptation in the United States: The Fourth National Climate Assessment, Volume II*. https://doi.org/10.7930/NCA4.2018.CH19

Census. (2010). *2010 Census: North Carolina Profile Population Density by Census Tract*. https://www2.census.gov/geo/maps/dc10_thematic/2010_Profile/2010_Profile_Map_North_Carolina.pdf

Census. (2021). *North Carolina Popoulation Change Between Census Decade*. U. S. Census Bureau. https://www.census.gov/library/stories/state-by-state/north-carolina-population-change-between-census-decade.html

Chai, T., & Draxler, R. R. (2014). Root mean square error (RMSE) or mean absolute error (MAE)? *Geosci. Model Dev. Discuss*, *7*, 1525–1534. https://doi.org/10.5194/gmdd-7-1525-2014

Chang, H. (2003). Basin Hydrologic Response to Changes in Climate and Land Use: The Conestoga River Basin, Pennsylvania. *Physical Geography*, *24*(3), 222–247. https://doi.org/10.2747/0272-3646.24.3.222

Chen, J., Theller, L., Gitau, M. W., Engel, B. A., & Harbor, J. M. (2017). Urbanization impacts on surface runoff of the contiguous United States. *Journal of Environmental Management*, *187*, 470–481. https://doi.org/10.1016/j.jenvman.2016.11.017

Chow, V., Maidment, D., & Mays, L. (1988). *Applied Hydrology*. McGraw-Hill.

Conroy, M. J., Allen, C. R., Peterson, J. T., Pritchard, L., & Moore, C. T. (2003). Landscape change in the Southern Piedmont: Challenges, solutions and uncertainty across scales. *Ecology and Society*, *8*(2). https://doi.org/10.5751/es-00598-080203

CRED. (2022). *2021 Disasters in numbers*. https://doi.org/10.1787/eee82e6e-en

Cuo, L., Beyene, T. K., Voisin, N., Su, F., Lettenmaier, D. P., Alberti, M., & Richey, J. E. (2011). Effects of mid-twenty-first century climate and land cover change on the hydrology of the Puget Sound basin, Washington. *Hydrological Processes*, *25*(11), 1729–1753. https://doi.org/10.1002/hyp.7932

Daniell, J., Wenzel, F., & Schaefer, A. (2016). The economic costs of natural disasters globally from 1900-2015: historical and normalised floods, storms, earthquakes, volcanoes, bushfires, drought and other disasters. *EGU General Assembly Conference Abstracts*, *1899*.

Davenport, F. v., Burke, M., & Diffenbaugh, N. S. (2021). Contribution of historical precipitation change to US flood damages. *Proceedings of the National Academy of Sciences of the United States of America*, *118*(4), 1–7. https://doi.org/10.1073/pnas.2017524118

DeCicco. (2021, January 8). *dataRetrieval Tutorial - Using R to Discover Data*. USGS.

Dethier, E. N., Sartain, S. L., Renshaw, C. E., & Magilligan, F. J. (2020). Spatially coherent regional changes in seasonal extreme streamflow events in the United States and Canada since 1950. *Science Advances*, *6*(49), 1–9. https://doi.org/10.1126/sciadv.aba5939

Dixon, K. W., Lanzante, J. R., Nath, M. J., Hayhoe, K., Stoner, A., Radhakrishnan, A., Balaji, V., & Gaitán, C. F. (2016). Evaluating the stationarity assumption in statistically downscaled climate projections: is past performance an indicator of future results? *Climatic Change*, *135*(3–4), 395–408. https://doi.org/10.1007/s10584-016-1598-0

Doll, B. A., Kurki-Fox, J. J., & Line, D. E. (2020). A framework for planning and evaluating the role of urban stream restoration for improving transportation resilience to extreme rainfall events. *Water (Switzerland)*, *12*(6). https://doi.org/10.3390/w12061620

Dottori, F., Alfieri, L., Rossi, L., Rudari, R., Ward, P. J., & Zhao, F. (2021). *Global River Flood Risk Under Climate Change*. 251–270. https://doi.org/10.1002/9781119427339.ch14

Dottori, F., Szewczyk, W., Ciscar, J. C., Zhao, F., Alfieri, L., Hirabayashi, Y., Bianchi, A., Mongelli, I., Frieler, K., Betts, R. A., & Feyen, L. (2018). Increased human and economic losses from river flooding with anthropogenic warming. *Nature Climate Change*, *8*(9), 781–786. https://doi.org/10.1038/S41558-018-0257-Z

Doubleday, G., Sebastian, A., Luttenschlager, T., & Bedient, P. B. (2013). Modeling Hydrologic Benefits of Low Impact Development: A Distributed Hydrologic Model of The Woodlands, Texas. *Journal of the American Water Resources Association*, *49*(6), 1444–1455. https://doi.org/10.1111/jawr.12095

Duque, F. Q., Villarini, G., Prein, A., Zhang, W., & Krajewski, W. (2022). Discharge and Floods Projected to Increase More Than Precipitation Extremes. *Hydrological Processes*.

Easterling, D., Arnold, J., Knutson, T., Kunkel, K. E., LeGrande, A. N., Leung, L. R., Vose, R. S., Waliser, D. E., & Wehner, M. F. (2017). *Ch. 7: Precipitation Change in the United States. Climate Science Special Report: Fourth National Climate Assessment, Volume I*. https://doi.org/10.7930/J0H993CC

EPA. (2017). U.S. Environmental Protection Agency. Updates To The Demographic And Spatial Allocation Models To Produce Integrated Climate And Land Use Scenarios (Iclus) (Final Report, Version 2). U.S. Environmental Protection Agency, Washington, DC, EPA/600/R-16/366F. *Report*, *January*.

Ercan, M. B., Maghami, I., Bowes, B. D., Morsy, M. M., & Goodall, J. L. (2020). Estimating Potential Climate Change Effects on the Upper Neuse Watershed Water Balance Using the SWAT Model. *Journal of the American Water Resources Association*, *56*(1), 53–67. https://doi.org/10.1111/1752-1688.12813

Exum, L. R., Bird, S. L., Harrison, J., & Perkins, C. a. (2005). *Estimating and Projecting Impervious Cover in the Southeastern United States*. *May*, 126.

Fagnant, C., Gori, A., Sebastian, A., Bedient, P. B., & Ensor, K. B. (2020). Characterizing spatiotemporal trends in extreme precipitation in Southeast Texas. *Natural Hazards*, *104*(2), 1597–1621. https://doi.org/10.1007/s11069-020-04235-x

Feldman, A. D. (2000). *Hydrologic modeling system HEC-HMS: technical reference manual*. US Army Corps of Engineers, Hydrologic Engineering Center.

Foley, J. A., DeFries, R., Asner, G. P., Barford, C., Bonan, G., Carpenter, S. R., Chapin, F. S., Coe, M. T., Daily, G. C., Gibbs, H. K., Helkowski, J. H., Holloway, T., Howard, E. A., Kucharik, C. J., Monfreda, C., Patz, J. A., Prentice, I. C., Ramankutty, N., & Snyder, P. K. (2005). Global consequences of land use. *Science*, *309*(5734), 570–574. https://doi.org/10.1126/science.1111772

Frey, W. H. (2012). *Putting the Volatile 2000s in Perspective " From a national*.

Gardner, L. R. (2009). Assessing the effect of climate change on mean annual runoff. *Journal of Hydrology*, *379*(3–4), 351–359. https://doi.org/10.1016/j.jhydrol.2009.10.021

Gori, A., Blessing, R., Juan, A., Brody, S., & Bedient, P. (2019a). Characterizing urbanization impacts on floodplain through integrated land use, hydrologic, and hydraulic modeling. *Journal of Hydrology*, *568*(October 2018), 82–95. https://doi.org/10.1016/j.jhydrol.2018.10.053

Gori, A., Blessing, R., Juan, A., Brody, S., & Bedient, P. (2019b). Characterizing urbanization impacts on floodplain through integrated land use, hydrologic, and hydraulic modeling. *Journal of Hydrology*, *568*(October 2018), 82–95. https://doi.org/10.1016/j.jhydrol.2018.10.053

Gregory, J., Kes, D., Jon es, P., & Miller, G. (2006). Effect of urban soil compaction on infiltration rate. *Journal of Soil and Water Conservation*, *61*(3), 117–123.

Gumbel, E. J. (1941). The Return Period of Flood Flows. In *Source: The Annals of Mathematical Statistics* (Vol. 12, Issue 2).

Güneralp, B., Güneralp, I., Liu, Y., Gü Neralp, B., & Nci Gü Neralp, I. ˙. (2015). Changing global patterns of urban exposure to flood and drought hazards Systems approach towards sustainable cities View project Global urban growth and its impact on biodiversity View project Changing global patterns of urban exposure to flood and drough. *Global Environmental Change*, *31*, 217–225. https://doi.org/10.1016/j.gloenvcha.2015.01.002

Gupta, A. sen, Jourdain, N. C., Brown, J. N., & Monselesan, D. (2013). Climate drift in the CMIP5 models. *Journal of Climate*, *26*(21), 8597–8615. https://doi.org/10.1175/JCLI-D-12-00521.1

Hagemeier-Klose, M., & Wagner, K. (2009). Evaluation of flood hazard maps in print and web mapping services as information tools in flood risk communication. In *Hazards Earth Syst. Sci* (Vol. 9). www.nat-hazards-earth-syst-sci.net/9/563/2009/

Hart, O. E., & Halden, R. U. (2019). On the need to integrate uncertainty into U.S. water resource planning. In *Science of the Total Environment* (Vol. 691, pp. 1262–1270). Elsevier B.V. https://doi.org/10.1016/j.scitotenv.2019.07.164

Hausfather, Z., & Peters, G. P. (2020). Emissions – the 'business as usual' story is misleading. *Nature*, *577*, 618–620.

Hawkins, E., & Sutton, R. (2009). The potential to narrow uncertainty in regional climate predictions. *Bulletin of the American Meteorological Society*, *90*(8), 1095–1107. https://doi.org/10.1175/2009BAMS2607.1

Hirabayashi, Y., Mahendran, R., Koirala, S., Konoshima, L., Yamazaki, D., Watanabe, S., Kim, H., & Kanae, S. (2013). Global flood risk under climate change. *Nature Climate Change*, *3*(9), 816–821. https://doi.org/10.1038/nclimate1911

Hodgkins, G. A., Whitfield, P. H., Burn, D. H., Hannaford, J., Renard, B., Stahl, K., Fleig, A. K., Madsen, H., Mediero, L., Korhonen, J., Murphy, C., & Wilson, D. (2017). Climate-driven variability in the occurrence of major floods across North America and Europe. *Journal of Hydrology*, *552*, 704–717. https://doi.org/10.1016/j.jhydrol.2017.07.027

Huang, H. J., Cheng, S. J., Wen, J. C., & Lee, J. H. (2008). Effect of growing watershed imperviousness on hydrograph parameters and peak discharge. *Hydrological Processes*, *22*(13), 2075–2085. https://doi.org/10.1002/hyp.6807

Huq, E., & Abdul-Aziz, O. I. (2021). Climate and land cover change impacts on stormwater runoff in large-scale coastal-urban environments. *Science of the Total Environment*, *778*, 146017. https://doi.org/10.1016/j.scitotenv.2021.146017

Hurtt, G. C., Chini, L. P., Frolking, S., Betts, R. A., Feddema, J., Fischer, G., Fisk, J. P., Hibbard, K., Houghton, R. A., Janetos, A., Jones, C. D., Kindermann, G., Kinoshita, T., Klein Goldewijk, K., Riahi, K., Shevliakova, E., Smith, S., Stehfest, E., Thomson, A., … Wang, Y. P. (2011). Harmonization of land-use scenarios for the period 1500-2100: 600 years of global gridded annual land-use transitions, wood harvest, and resulting secondary lands. *Climatic Change*, *109*(1), 117–161. https://doi.org/10.1007/s10584-011-0153-2

IPCC. (2007). *Report of the 26th session of the IPCC*.

Juan, A., Gori, A., & Sebastian, A. (2020). Comparing floodplain evolution in channelized and unchannelized urban watersheds in Houston, Texas. *Journal of Flood Risk Management*, *13*(2). https://doi.org/10.1111/jfr3.12604

Kalyanapu, A. J., Burian, S. J., & Mcpherson, T. N. (2009). Effect of land use-based surface roughness on hydrologic model output. In *Journal of Spatial Hydrology* (Vol. 9, Issue 2).

Kaushal, S. S., Gold, A. J., & Mayer, P. M. (2017). Land use, climate, and water resources-global stages of interaction. In *Water (Switzerland)* (Vol. 9, Issue 10, p. 815). MDPI AG. https://doi.org/10.3390/w9100815

Kiem, A. S., & Verdon-Kidd, D. C. (2013). The importance of understanding drivers of hydroclimatic variability for robust flood risk planning in the coastal zone. *Australian Journal of Water Resources*, *17*(2), 126–134. https://doi.org/10.7158/W13-015.2013.17.2

Knutti, R., & Sedláček, J. (2013). Robustness and uncertainties in the new CMIP5 climate model projections. *Nature Climate Change*, *3*(4), 369–373. https://doi.org/10.1038/nclimate1716

Koutsoyiannis, D. (2003). On the appropriateness of the gumbel distribution in modelling extreme rainfall. *Water*, *October 2003*, 303–319. https://doi.org/10.13140/RG.2.1.3811.6080

Kundzewicz, Z. W., Su, B., Wang, Y., Wang, G., Wang, G., Huang, J., & Jiang, T. (2019). Flood risk in a range of spatial perspectives - From global to local scales. *Natural Hazards and Earth System Sciences*, *19*(7), 1319–1328. https://doi.org/10.5194/nhess-19-1319-2019

Kunkel, K. E., Easterling, D. R., Ballinger, A., Bililign, S., Champion, S. M., Corbett, D. R., Dello, K. D., Dissen, J., Lackmann, G. M., Luettich, R. A. Jr., Perry, L. B., Robinson, W. A., Stevens, L. E., Stewart, B. C., & Terando, A. J. (2020). North Carolina Climate Science Report. *North Carolina Institute for Climate Studies*, 233 p.

Lafontaine, J. H., Hay, L. E., Viger, R. J., Regan, R. S., & Markstrom, S. L. (2015). Effects of Climate and Land Cover on Hydrology in the Southeastern U.S.: Potential Impacts on Watershed Planning. *Journal of the American Water Resources Association*, *51*(5), 1235–1261. https://doi.org/10.1111/1752-1688.12304

Latto, A., Hagen, A., & Berg, R. (2021). *National Hurricane Center Tropical Cyclone Report: Hurricane Isaias (AL092020)*.

Lawler, J. J., Lewis, D. J., Nelson, E., Plantinga, A. J., Polasky, S., Withey, J. C., Helmers, D. P., Martinuzzi, S., Penningtonh, D., & Radeloff, V. C. (2014). Projected land-use change impacts on ecosystem services in the United States. *Proceedings of the National Academy of Sciences of the United States of America*, *111*(20), 7492–7497. https://doi.org/10.1073/pnas.1405557111

Lighthill, F., & Whitham, G. (1950). On Kinematic Waves, I, Flood Measurements in Long Rivers. *Proceedings of the Royal Society of London*, *229*, 281–316.

Liu, Z., Mehran, A., Phillips, T. J., & AghaKouchak, A. (2014). Seasonal and regional biases in CMIP5 precipitation simulations. *Climate Research*, *60*(1), 35–50. https://doi.org/10.3354/cr01221

Livneh, B., Rosenberg, E. A., Lin, C., Nijssen, B., Mishra, V., Andreadis, K. M., Maurer, E. P., & Lettenmaier, D. P. (2013). A long-term hydrologically based dataset of land surface fluxes and states for the conterminous United States: Update and extensions. *Journal of Climate*, *26*(23), 9384–9392. https://doi.org/10.1175/JCLI-D-12-00508.1

Markonis, Y., & Koutsoyiannis, D. (2016). Scale-dependence of persistence in precipitation records. *Nature Climate Change*, *6*(4), 399–401. https://doi.org/10.1038/nclimate2894

Martin, K. L., Hwang, T., Vose, J. M., Coulston, J. W., Wear, D. N., Miles, B., & Band, L. E. (2017). Watershed impacts of climate and land use changes depend on magnitude and land use context. *Ecohydrology*, *10*(7), 1–17. https://doi.org/10.1002/eco.1870

Mccuen, R. H., Knight, Z., & Cutter, A. G. (2006). Evaluation of the Nash-Sutcliffe Efficiency Index. *Journal of Hydrologic Engineering*, *11*(6), 597–602. https://doi.org/10.1061/ASCE1084-0699200611:6597

Meitzen, K. M. (2016). Stream flow changes across North Carolina (USA) 1955–2012 with implications for environmental flow management. *Geomorphology*, *252*, 171–184. https://doi.org/10.1016/J.GEOMORPH.2015.06.019

Milly, P. C. D., Betancourt, J., Falkenmark, M., Hirsch, R. M., Kundzewicz, Z. W., Lettenmaier, D. P., & Stouffer, R. J. (2008). Climate change: Stationarity is dead: Whither water management? *Science*, *319*(5863), 573–574. https://doi.org/10.1126/science.1151915

Mohanty, M. P., & Simonovic, S. P. (2021). Changes in floodplain regimes over Canada due to climate change impacts: Observations from CMIP6 models. *Science of the Total Environment*, *792*, 148323. https://doi.org/10.1016/j.scitotenv.2021.148323

Mojtahedi, M., & Oo, B. L. (2017). Critical attributes for proactive engagement of stakeholders in disaster risk management. In *International Journal of Disaster Risk Reduction* (Vol. 21, pp. 35–43). Elsevier Ltd. https://doi.org/10.1016/j.ijdrr.2016.10.017

NCOSBM. (2022). *Projected Population of the State of North Carolina and Its Counties July 1, 2021 - July 1, 2050*. https://www.osbm.nc.gov/media/1547/download?attachment

NWS. (2019). *Post Tropical Cyclone Report: Hurricane Dorian*.

O'Donnell, E. C., & Thorne, C. R. (2020). Drivers of future urban flood risk. *Philosophical Transactions of the Royal Society A: Mathematical, Physical and Engineering Sciences*, *378*(2168). https://doi.org/10.1098/rsta.2019.0216

O'Driscoll, M., Clinton, S., Jefferson, A., Manda, A., & McMillan, S. (2010). Urbanization effects on watershed hydrology and in-stream processes in the southern United States. In *Water (Switzerland)* (Vol. 2, Issue 3, pp. 605–648). MDPI AG. https://doi.org/10.3390/w2030605

Ogden, F. L., Raj Pradhan, N., Downer, C. W., & Zahner, J. A. (2011). Relative importance of impervious area, drainage density, width function, and subsurface storm drainage on flood runoff from an urbanized catchment. *Water Resources Research*, *47*(12). https://doi.org/10.1029/2011WR010550

O'Neill, B. C., Kriegler, E., Riahi, K., Ebi, K. L., Hallegatte, S., Carter, T. R., Mathur, R., & van Vuuren, D. P. (2014). A new scenario framework for climate change research: The concept of shared socioeconomic pathways. *Climatic Change*, *122*(3), 387–400. https://doi.org/10.1007/s10584-013-0905-2

Paerl, H. W., Hall, N. S., Hounshell, A. G., Rossignol, K. L., Barnard, M. A., Luettich, R. A., Rudolph, J. C., Osburn, C. L., Bales, J., & Harding, L. W. (2020). Recent increases of rainfall and flooding from tropical cyclones (TCs) in North Carolina (USA): implications for organic matter and nutrient cycling in coastal watersheds. *Biogeochemistry*, *150*(2), 197–216. https://doi.org/10.1007/s10533-020-00693-4

Pokhrel, I., Kalra, A., Rahaman, M. M., & Thakali, R. (2020). Forecasting of Future Flooding and Risk Assessment under CMIP6 Climate Projection in Neuse River, North Carolina. *Forecasting*, *2*(3), 323–345. https://doi.org/10.3390/forecast2030018

Pörtner, H. O., Roberts, D. C., Adams, H., Adler, C., Aldunce, P., Ali, E., & Ara Begum, R. (2022). *Climate change 2022: impacts, adaptation and vulnerability*.

Prestele, R., Alexander, P., Rounsevell, M. D. A., Arneth, A., Calvin, K., Doelman, J., Eitelberg, D. A., Engström, K., Fujimori, S., Hasegawa, T., Havlik, P., Humpenöder, F., Jain, A. K., Krisztin, T., Kyle, P., Meiyappan, P., Popp, A., Sands, R. D., Schaldach, R., … Verburg, P. H. (2016). Hotspots

of uncertainty in land-use and land-cover change projections: a global-scale model comparison. *Global Change Biology*, *22*(12), 3967–3983. https://doi.org/10.1111/gcb.13337

Pricope, N. G., Hidalgo, C., Pippin, J. S., & Evans, J. M. (2022). Shifting landscapes of risk: Quantifying pluvial flood vulnerability beyond the regulated floodplain. *Journal of Environmental Management*, *304*(November 2021). https://doi.org/10.1016/j.jenvman.2021.114221

Pumo, D., Arnone, E., Francipane, A., Caracciolo, D., & Noto, L. v. (2017). Potential implications of climate change and urbanization on watershed hydrology. *Journal of Hydrology*, *554*, 80–99. https://doi.org/10.1016/j.jhydrol.2017.09.002

Rawls, W. J., Asce, M., Brakensiek, D. L., & Miller, N. (1983). GREEN-AMPT INFILTRATION PARAMETERS FROM SOILS DATA. *Journal of Hydraulic Engineering*, *109*(1), 62–70.

Reidmiller, D., Avery, C., Easterling, D., Kunkel, K., & Lewis, K. (2018). Fourth National Climate Assessment: Report-in-Brief. *Washington, DC: US Glob. Change Red. Program*, *II*, 1–470.

Rogger, M., Agnoletti, M., Alaoui, A., Bathurst, J. C., Bodner, G., Borga, M., Chaplot, V., Gallart, F., Glatzel, G., Hall, J., Holden, J., Holko, L., Horn, R., Kiss, A., Quinton, J. N., Leitinger, G., Lennartz, B., Parajka, J., Peth, S., … Viglione, A. (2017). Land use change impacts on floods at the catchment scale: Challenges and opportunities for future research. *Water Resources Research*, *June 2013*, 5209–5219. https://doi.org/10.1002/2017WR020723.Received

Rothenberger, M. B., Burkholder, J. M., & Brownie, C. (2009). Long-term effects of changing land use practices on surface water quality in a coastal river and lagoonal estuary. *Environmental Management*, *44*(3), 505–523. https://doi.org/10.1007/s00267-009-9330-8

Schulz, K., & Bernhardt, M. (2016). The end of trend estimation for extreme floods under climate change? *Hydrological Processes*, *30*(11), 1804–1808. https://doi.org/10.1002/hyp.10816

Schwalm, C. R., Glendon, S., & Duffy, P. B. (2020). RCP8.5 tracks cumulative CO2 emissions. *Proceedings of the National Academy of Sciences of the United States of America*, *117*(33), 19656–19657. https://doi.org/10.1073/PNAS.2007117117

Sebastian, A., Gori, A., Blessing, R. B., van der Wiel, K., & Bass, B. (2019). Disentangling the impacts of human and environmental change on catchment response during Hurricane Harvey. *Environmental Research Letters*, *14*(12). https://doi.org/10.1088/1748-9326/ab5234

Shepherd, J. M. (2005). A review of current investigations of urban-induced rainfall and recommendations for the future. *Earth Interactions*, *9*(12). https://doi.org/10.1175/EI156.1

Slater, L., & Villarini, G. (2016). Recent trends in U.S. flood risk. *Geophysical Research Letters*, *43*(24), 12,428-12,436. https://doi.org/10.1002/2016GL071199

Slater, L., Villarini, G., Archfield, S., Faulkner, D., Lamb, R., Khouakhi, A., & Yin, J. (2021). Global Changes in 20-Year, 50-Year, and 100-Year River Floods. *Geophysical Research Letters*, *48*(6), 1–10. https://doi.org/10.1029/2020GL091824

Sohl, T. L., Wimberly, M. C., Radeloff, V. C., Theobald, D. M., & Sleeter, B. M. (2016). Divergent projections of future land use in the United States arising from different models and scenarios. *Ecological Modelling*, *337*, 281–297. https://doi.org/10.1016/j.ecolmodel.2016.07.016

Sridhar, V., Modi, P., Billah, M. M., Valayamkunnath, P., & Goodall, J. L. (2019). Precipitation Extremes and Flood Frequency in a Changing Climate in Southeastern Virginia. *Journal of the American Water Resources Association*, *55*(4), 780–799. https://doi.org/10.1111/1752-1688.12752

Steinschneider, S., McCrary, R., Mearns, L. O., & Brown, C. (2015). The effects of climate model similarity on probabilistic climate projections and the implications for local, risk-based adaptation planning. *Geophysical Research Letters*, *42*(12), 5014–5022. https://doi.org/10.1002/2015GL064529

Stewart, S. R. (2017). National Hurricane Center Tropical Cyclone Report: Hurricane Matthew (AL142016). In *National Hurricane Center* (Issue October 2016). http://www.nhc.noaa.gov/data/tcr/AL142016_Matthew.pdf

Stewart, S. R., & Berg, R. (2019). National Hurricane Center Tropical Cyclone Report: Hurricane Florence (AL062018). In *National Hurricane Center* (Issue May). https://www.nhc.noaa.gov/data/tcr/AL152017_Maria.pdf

Strengers, B., Leemans, R., Eickhout, B., de Vries, B., & Bouwman, L. (2004). The land-use projections and resulting emissions in the IPCC SRES scenarios as simulated by the IMAGE 2.2 model. *GeoJournal*, *61*, 381–393.

Sunde, M. G., He, H. S., Hubbart, J. A., & Urban, M. A. (2018). An integrated modeling approach for estimating hydrologic responses to future urbanization and climate changes in a mixed-use midwestern watershed. *Journal of Environmental Management*, *220*, 149–162. https://doi.org/10.1016/j.jenvman.2018.05.025

Sun, G., Mcnulty, S. G., Amatyabtc, D. M., Skaggsb3, R. W., Swift, L. W., Shepard, J. P., & Riekerkf, H. (2002). A comparison of the watershed hydrology of coastal forested wetlands and the mountainous uplands in the Southern US. In *Journal of Hydrology* (Vol. 263). www.elsevier.comkxate/jhydrol

Suriya, S., & Mudgal, B. v. (2012). Impact of urbanization on flooding: The Thirusoolam sub watershed - A case study. *Journal of Hydrology*, *412–413*, 210–219. https://doi.org/10.1016/j.jhydrol.2011.05.008

Suttles, K. M., Singh, N. K., Vose, J. M., Martin, K. L., Emanuel, R. E., Coulston, J. W., Saia, S. M., & Crump, M. T. (2018). Assessment of hydrologic vulnerability to urbanization and climate change in a rapidly changing watershed in the Southeast U.S. *Science of the Total Environment*, *645*, 806–816. https://doi.org/10.1016/j.scitotenv.2018.06.287

Swain, D. L., Wing, O. E. J., Bates, P. D., Done, J. M., Johnson, K. A., & Cameron, D. R. (2020). Increased Flood Exposure Due to Climate Change and Population Growth in the United States. *Earth's Future*, *8*(11). https://doi.org/10.1029/2020EF001778

Terando, A. J., Costanza, J., Belyea, C., Dunn, R. R., & Mckerrow, A. (2014). The Southern Megalopolis: Using the Past to Predict the Future of Urban Sprawl in the Southeast. *PLoS ONE*, *9*(7), 102261. https://doi.org/10.1371/journal.pone.0102261

Tong, S. T. Y., Yang, H., Chen, H., & Yang, J. Y. (2016). Hydrologic impacts of climate change and urbanization in the Las Vegas Wash Watershed, Nevada. *Journal of Water and Climate Change*, *7*(3), 598–620. https://doi.org/10.2166/wcc.2016.038

Turner, D. P., Conklin, D. R., & Bolte, J. P. (2015). Projected climate change impacts on forest land cover and land use over the Willamette River Basin, Oregon, USA. *Climatic Change*, *133*(2), 335–348. https://doi.org/10.1007/s10584-015-1465-4

USACE. (2013). *Falls Lake Master Plan Neuse River Basin*.

USACE. (2016). *HEC-RAS River Analysis System*.

USACE. (2018, November 13). *Wilmington District Responds to Hurricane Florence*. US Army Corps of Engineers Wilmington District Website.

USDA. (1986). *Urban Hydrology for Small Watersheds TR-55*.

U.S. EPA. (2017). *Updates To The Demographic And Spatial Allocation Models To Produce Integrated Climate And Land Use Scenarios (Iclus) (Final Report, Version 2)*.

Vieux, B. E., Cui, Z., & Guar, A. (2004). Evaluation of a PhysicsBased Distributed Hydrologic Model for Flood Forecasting. *Journal of Hydrology*, *298*(1–4), 155–177.

Walsh, C. J., Roy, A. H., Feminella, J. W., Cottingham, P. D., Groffman, P. M., & Morgan, R. P. (2005). The urban stream syndrome: Current knowledge and the search for a cure. *Journal of the North American Benthological Society*, *24*(3), 706–723. https://doi.org/10.1899/04-028.1

Wang, C., Zhang, L., Lee, S. K., Wu, L., & Mechoso, C. R. (2014). A global perspective on CMIP5 climate model biases. *Nature Climate Change*, *4*(3), 201–205. https://doi.org/10.1038/nclimate2118

Wang, R., Kalin, L., Kuang, W., & Tian, H. (2014). Individual and combined effects of land use/cover and climate change on Wolf Bay watershed streamflow in southern Alabama. *Hydrological Processes*, *28*(22), 5530–5546. https://doi.org/10.1002/hyp.10057

Wear, D. N. (2013). *Forecasts of Land Use* (Vol. 178).

West, T. O., le Page, Y., Huang, M., Wolf, J., & Thomson, A. M. (2014). Downscaling global land cover projections from an integrated assessment model for use in regional analyses: Results and evaluation for the US from 2005 to 2095. *Environmental Research Letters*, *9*(6). https://doi.org/10.1088/1748-9326/9/6/064004

Wing, O., Bates, P. D., Smith, A. M., Sampson, C. C., Johnson, K. A., Fargione, J., & Morefield, P. (2018). Estimates of present and future flood risk in the conterminous United States. *Environmental Research Letters*, *13*(3). https://doi.org/10.1088/1748-9326/aaac65

Wing, O., Lehman, W., Bates, P., Sampson, C., & Quinn, N. (2022). U . S . flood risk in the Anthropocene. *Nature Climate Change*, *12*(2), 156–162.

Winsemius, H. C., Aerts, J. C. J. H., van Beek, L. P. H., Bierkens, M. F. P., Bouwman, A., Jongman, B., Kwadijk, J. C. J., Ligtvoet, W., Lucas, P. L., van Vuuren, D. P., & Ward, P. J. (2016). Global drivers of future river flood risk. *Nature Climate Change*, *6*(4), 381–385. https://doi.org/10.1038/nclimate2893

Ye, B., Jiang, J., Liu, J., Zheng, Y., & Zhou, N. (2021). Research on quantitative assessment of climate change risk at an urban scale: Review of recent progress and outlook of future direction. In *Renewable and Sustainable Energy Reviews* (Vol. 135). Elsevier Ltd. https://doi.org/10.1016/j.rser.2020.110415

Yi, A. (2021). Personal Communications. In *Neuse River Flood Mitigation Study HMS Model - Dam Locations*.

Yuan, N., Huang, Y., Duan, J., Zhu, C., Xoplaki, E., & Luterbacher, J. (2019). On climate prediction: how much can we expect from climate memory? *Climate Dynamics*, *52*(1–2), 855–864. https://doi.org/10.1007/s00382-018-4168-5

Yue, S., Ouarda, T. B. M. J., Bobée, B., Legendre, P., & Bruneau, P. (1999). The Gumbel mixed model for flood frequency analysis. *Journal of Hydrology*, *226*(1–2), 88–100. https://doi.org/10.1016/S0022-1694(99)00168-7

Zhao, G., Gao, H., & Cuo, L. (2016). Effects of urbanization and climate change on peak flows over the San Antonio River basin, Texas. *Journal of Hydrometeorology*, *17*(9), 2371–2389. https://doi.org/10.1175/JHM-D-15-0216.1

Zuellig, R. E., Bruce, J. F., Evans, E. E., & Stogner, R. W. (2008). Urban-Related Environmental Variables and Their Relation with Patterns in Biological Community Structure in the Fountain Creek Basin , Colorado , 2003 – 2005 Scientific Investigations Report 2007 – 5225. *Engineering*, 24.